THE JOURNAL OF BIOLOGICAL CHEMISTRY VOL. 286, NO. 29, pp. 25903–25921, July 22, 2011

Skeletal Muscle Differentiation and Fusion Are Regulated by the BAR-containing Rho-GTPase-activating Protein (Rho-GAP), GRAF1*[S]

Received for publication, March 23, 2011, and in revised form, May 23, 2011 Published, JBC Papers in Press, May 26, 2011, DOI 10.1074/jbc.M111.243030

Jason T. Doherty[‡1], Kaitlin C. Lenhart[‡2], Morgan V. Cameron[‡], Christopher P. Mack[‡§], Frank L. Conlon[§¶‖], and Joan M. Taylor[‡§3]

From the Departments of [‡]Pathology and Laboratory Medicine, [¶]Biology, and [‖]Genetics, [§]McAllister Heart Institute, University of North Carolina, Chapel Hill, North Carolina 27599

Although RhoA activity is necessary for promoting myogenic mesenchymal stem cell fates, recent studies in cultured cells suggest that down-regulation of RhoA activity in specified myoblasts is required for subsequent differentiation and myotube formation. However, whether this phenomenon occurs *in vivo* and which Rho modifiers control these later events remain unclear. We found that expression of the Rho-GTPase-activating protein, GRAF1, was transiently up-regulated during myogenesis, and studies in C2C12 cells revealed that GRAF1 is necessary and sufficient for mediating RhoA down-regulation and inducing muscle differentiation. Moreover, forced expression of GRAF1 in pre-differentiated myoblasts drives robust muscle fusion by a process that requires GTPase-activating protein-dependent actin remodeling and BAR-dependent membrane binding or sculpting. Moreover, morpholino-based knockdown studies in *Xenopus laevis* determined that GRAF1 expression is critical for muscle development. GRAF1-depleted embryos exhibited elevated RhoA activity and defective myofibrillogenesis that resulted in progressive muscle degeneration, defective motility, and embryonic lethality. Our results are the first to identify a GTPase-activating protein that regulates muscle maturation and to highlight the functional importance of BAR domains in myotube formation.

Skeletal muscle development is a tightly regulated process involving the specification of mesodermal precursors into myoblasts and subsequent differentiation and fusion of these cells into multinucleated myotubes. Primary myogenesis is initiated in somites via the spatial and temporal expression of myogenic regulatory factors that include MyoD and Myf5, which are required for initial specification of skeletal myoblasts, and myogenin, MRF4, and myocyte-specific enhancer factors (MEF2a and MEF2c), which induce differentiation of these specified cells. Additional transcriptional control of skeletal muscle differentiation is imparted by serum-response factor, a MADS box-containing transcription factor that promotes both myoblast proliferation and expression of skeletal muscle marker genes (for review see Ref. 1).

It is not completely clear how these myogenic regulatory factors are activated during development, but it is known that the small GTPase Rho (which can induce serum-response factor-dependent gene transcription) plays a role. RhoA was reported to both promote and interfere with the skeletal muscle differentiation program (for review see Ref. 2). However, more recent studies in cultured cells suggest that RhoA activity must be tightly regulated in a finely coordinated time-dependent manner to ensure appropriate skeletal muscle formation (3–5). Specifically, these later studies showed that although RhoA activity is necessary for specification of myoblasts, down-regulation of RhoA activity in specified myoblasts is essential for subsequent cell cycle withdrawal, expression of skeletal muscle differentiation genes, and myotube fusion (*i.e.* secondary myogenesis). The mechanism by which down-regulation of Rho promotes skeletal muscle differentiation appears to be due to the fact that RhoA-dependent activation of MRTF-A in proliferating myoblasts induces the expression of the transcriptional inhibitor, Id3. Id3, which has a helix-loop-helix domain but lacks a DNA binding domain, blocks the function of myogenic regulatory factors by forming transcriptionally inactive complexes or by competing for E protein binding (6). Importantly, Iwasaki *et al.* (4) found that depletion of Id3 in proliferating C2C12 cells induced terminal differentiation.

Secondary myogenesis occurs through the fusion of singly nucleated myoblasts into multinucleated myotubes, a process that also requires down-regulation of RhoA (3). Although a complete understanding of the mechanisms governing skeletal muscle fusion is lacking, it is clear that dramatic reorganization of the cytoskeleton occurs during this dynamic process (7). In particular, previous studies have revealed that the formation and subsequent dissolution of an F-actin focus at the distal ends of fusion-competent myoblasts are essential for myoblast-myoblast fusion (8). Thus, tight control of Rho-dependent actin dynamics is likely important for this process.

Small GTPase activity is regulated by factors that facilitate the transition between an active GTP-bound state and an inac-

* This work was supported, in whole or in part, by National Institutes of Health Grants HL-081844 and HL-071054 (to J. M. T.), HL-070953 (to C. P. M.), and HL-089641 (to F. L. C.) from NHLBI and by Grant DE-018825 (to F. L. C.) from NIDCR. This work was also supported by American Heart Association Grants 0355776U (to J. M. T.) and 0555476U (to C. P. M.).

[S] The on-line version of this article (available at http://www.jbc.org) contains supplemental Figs. 1–8, Table 1, and Movies 1 and 2.

[1] Trainee in the Integrative Vascular Biology Program supported by National Institutes of Health Grant T32HL69768.

[2] Trainee in the Developmental Biology Program supported by National Institutes of Health Grant T32 HD046369-05.

[3] To whom correspondence should be addressed: University of North Carolina, CB7525 Chapel Hill, NC 27599. Fax: 919-966-6718; E-mail: jmt3x@med.unc.edu.

tive GDP-bound state. Restricted expression and subcellular localization of guanine nucleotide exchange proteins and GTPase-activating proteins (GAPs)[4] are thought to be important for precise spatial-temporal activation and inactivation of specific small GTPases (9). Previous studies have shown that p190B Rho-GAP expression in mesenchymal cells favors adipocyte specification over myogenic specification (10). However, to date, no Rho-GAPs have been identified that regulate muscle maturation. We previously cloned and characterized a multidomain containing Rho-specific GAP termed GRAF1. Interestingly, we found that GRAF1 associates with focal adhesion kinase (FAK) through an SH3 domain protein-protein interaction (11–13). Because FAK (a critical mediator of matrix and growth factor-dependent signaling), like Rho, has also been implicated in regulating muscle development (14–17), we reasoned that GRAF1 might serve as a key regulator of RhoA activity during myogenesis.

Using cultured mammalian myoblasts, we established that GRAF1 regulates skeletal muscle differentiation in a Rho-GAP-dependent and cell-autonomous fashion that requires its SH3 domain. Moreover, we show that GRAF1 expression drives muscle fusion by a process that requires GAP-dependent actin remodeling. Interestingly, GRAF1 also contains an amphipathic lipid bending/sculpting BAR domain, and we found that this domain is also critical for GRAF1-dependent muscle fusion *in vitro*. Furthermore, we show that GRAF1 is a *bona fide* modulator of Rho activity *in vivo* and that GRAF1 depletion in *Xenopus laevis* attenuates muscle maturation and leads to progressive myofiber degeneration. Our results are the first to identify a Rho-GAP that regulates muscle maturation and to highlight the functional importance of BAR domains in myotube formation.

EXPERIMENTAL PROCEDURES

Commercial Antibodies and cDNA Constructs—Antibodies used were ERK-CT (Upstate), myosin heavy chain (MHC, Abcam), skeletal α-actin (SKA, Sigma), α-actinin (Sigma), troponin T (CT3, Developmental Studies Hybridoma Bank), tropomyosin (CH1, Developmental Studies Hybridoma Bank), 12-101 (Developmental Studies Hybridoma Bank), HNK (ZN12; Developmental Studies Hybridoma Bank), and p21 (Santa Cruz Biotechnology). *Xenopus* and human *GRAF1* cDNAs were obtained from Open Biosystems and were directionally subcloned into cDNA3.1-FLAG or pRK5-Myc epitope-tagged vectors using 5′-BamHI and 3′-EcoRI restriction sites that were generated by PCR. Prk5 vectors containing constitutively active RhoA (L63) or dominant-negative RhoA (N19) were the generous gifts from Alan Hall, University College, London, United Kingdom). GAPm, BARm, and ΔBAR variants were generated by PCR site-directed mutagenesis using primers that were 5′-phosphorylated and HPLC-purified using standard procedures (QuickChange, Stratagene). To generate GRAF1^{loxP}, GAP^{loxP}, and ΔBAR^{loxP}, L63RhoA^{loxP} and N19RhoA^{loxP}, the Myc-tagged variants were amplified from pRK5myc− constructs by PCR with primers that incorporated 3′- and 5′-NotI sites with an internal KpnI site. This fragment was then ligated into a vector containing a cassette in which a 1700-bp fragment of the β-actin promoter was fused to cDNA containing GFP flanked by loxP sites (18). All constructs that were generated by PCR were confirmed by sequencing the entire coding sequence. Ad5CMV Cre adenovirus was purchased from the University of Iowa Gene Transfer Vector Core, and Ad5CMV LacZ adenovirus was purchased the University of North Carolina Chapel Hill Viral Core. Both viruses were expanded using Adenopure® adenovirus purification kit (Puresyn, Inc.) according to manufacturer's protocol.

Generation of GRAF1 Polyclonal Antibody—Amino acid sequences of human, mouse, and *X. laevis* GRAF1 were aligned, and the conserved sequence CGTLNGKTGLIPENYVEFL corresponding to the extreme C terminus of GRAF1 was selected for antibody production. Purified peptides were obtained commercially (Invitrogen), and rabbit polyclonal antibodies were generated commercially by standard procedures (Cocalico Biologicals). Sera were screened for immunoreactivity by Western analysis of lysates generated from COS cells transfected with plasmids encoding human or *Xenopus* GRAF1 and endogenous GRAF1 isolated from mouse heart and brain. A consistent band of the predicted 110-kDa size was also confirmed by Western analysis using *in vitro* translation assays utilizing recombinant human and *Xenopus* GRAF1 (supplemental Fig. S4, *A* and *B*). GRAF1 often appears as a doublet in skeletal muscle consistent with our previous studies in isolated cardiomyocytes (12). Although the origin of these two forms is not currently known, they could arise from either alternative transcripts or phosphorylation.

Morpholinos, Embryo Culture, and Microinjection—The following morpholinos conjugated to fluorescein isothiocyanate (FITC), and a standard control morpholino (Con Mo) were obtained from GeneTools. Sequences used were as follows: mo1, 5′ ACGAGATCAGGAAGGCATTGACA 3′, and mo2, 5′ GGTAATCCCATCCTGGCGTATAGCA 3′. Five-base mismatched morpholinos were designed for both mo1 and mo2 (5′ ACcAGATgAGcAAGcCATTcACA 3′ and 5′ GcTAATgCCATgCTGGCcTATAcCA 3′) and were used as controls to assess the specificity of the morphant phenotype. Preparation and injection of *X. laevis* embryos was carried out as described previously (19). Equal concentrations of mo1 and mo2 morpholinos (or mis-matched controls) were mixed and injected at a concentration of 40 ng/embryo at the one-cell stage (see supplemental Fig. S6 for efficacy and specificity of morpholinos).

In Vitro Transcription/Translation Assays—*In vitro* transcription/translation assays were performed on plasmids encoding *Xenopus GRAF1* and human *GRAF1* using the TnT Quick-coupled Transcription/Translation System according to the manufacturer's instructions (Promega).

Whole-mount Immunohistochemistry, TEM, and in Situ Hybridization—Embryos were prepared for whole-mount immunohistochemistry or TEM by fixation overnight at 4 °C in 4% or 2% paraformaldehyde plus 2.5% glyceraldehyde, respectively, and processed by standard procedures. In brief, for

[4] The abbreviations used are: GAP, GTPase-activating protein; Rho-GAP, Rho-GTPase-activating protein; TEM, transmission electron microscope; Tm, tropomyosin; FAK, focal adhesion kinase; LSM, low serum medium; SH3, Src homology domain 3; Mo, morpholino; Con Mo, control morpholino; SKA, skeletal α-actin.

immunohistochemistry, paraformaldehyde-fixed embryos were washed twice in PBS, 1% Triton X-100, 1% DMSO (PBS-TD) and were blocked for 4 h at room temperature in PBS-TD containing 0.1 M glycine, 2% powdered milk, and 5% goat serum. Embryos were photobleached in 5% H_2O_2 in PBS for at least 4 h under bright light. Embryos were then rinsed with PBS and treated with 1 μg/ml bovine testicular hyaluronidase in 50 mM sodium acetate buffer for 45 min at room temperature. Embryos were rinsed, blocked, and incubated overnight at 4 °C with primary antibodies diluted 1:200 in block buffer. Embryos were then washed six times (1 h each) in PBS-TD at room temperature and incubated overnight at 4 °C with the appropriate Cy-3 or Alexa-488 conjugated secondary antibodies (1:250) and ToPro3 (1:1000) to stain nuclei (Molecular Probes). Embryos were again washed six times (1 h each) in PBS-TD, fixed in Dent's fixative, and stored in 100% methanol at 20 °C.

Whole-mount *in situ* hybridization was performed as described previously (20). Plasmids for MyoD and xGRAF1 were linearized and used to generate digoxigenin-UTP-labeled (Roche Applied Science) antisense RNA probes using the appropriate restriction endonuclease and polymerase. Color detection was determined by BM Purple substrate (Roche Applied Science) after incubation with alkaline phosphatase-conjugated anti-digoxigenin antibody. For cryosectioning, embryos were incubated overnight at 4 °C in a 30% sucrose solution in PBS and embedded in Tissue Tek OCT (Sakura Finetek). Cryosections (14 μm) were cut on a Leica cryostat.

For TEM, stage 25 and 37 embryos were fixed in 2% paraformaldehyde and 2.5% glyceraldehyde overnight at 4 °C. Embryos were then processed and visualized by TEM as described previously (21). Briefly, embryos were post-fixed in ferrocyanide-reduced osmium and embedded in Spurr's epoxy resin. Parasagittal ultra-thin (70 nm) sections were mounted on copper grids and post-stained with 4% aqueous uranyl acetate followed by Reynold's lead citrate. Sections were imaged with a LEO EM-910 transmission electron microscope.

Microscopy and Image Deconvolution—Embryos were cleared for microscopic analysis in 2:1 benzyl benzoate/benzyl alcohol and placed on a glass coverslip. Embryos or cells were analyzed by wide field microscopy using a Leica MZFLIII fluorescence dissecting scope or Olympus IX81 microscope or by confocal microscopy using an Olympus FV500 laser-scanning confocal microscope. Images were acquired using a CoolSNAPfx CCD camera (Photometrics) and analyzed by ISEE, AMARIS, or Fluoview version 5.1 software. Confocal Z-stacks were obtained using a 1.24-μm step size. Z-series stacks were deconvolved using Autodeblur Gold version X.1.4.1 software (Autoquant, Media Cybernetics). RGB image overlays were performed using Adobe Photoshop.

Cell Culture, Transfection, and siRNA Treatment—The C2C12 mouse and L6 rat myoblast cell lines were obtained from ATCC and cultured at subconfluent density in growth media (G) consisting of Dulbecco's modified Eagle's media + 10% FBS + penicillin/streptomycin. For differentiation, myoblasts were plated on slides or dishes pre-coated with rat tail collagen (10 μg/ml) and transferred to low serum media (LSM) containing 2% horse serum. Cells maintained in growth media were transfected with cDNAs using Trans-IT (Mirus) transfection reagents according to the manufacturer's protocol. Cells were infected with Cre or LacZ adenoviruses at 100 multiplicities of infection.

Short interfering RNA (siRNA) oligonucleotides were obtained from Invitrogen with the following sequences: GCAGCUGUUGGCCUAUAAU(dT)(dT) and AUUAUAGGCCAACAGCUGC. C2C12 cells maintained in growth conditions (10% FCS) were transfected with 150 nM control or GRAF1-specific siRNAs according to the manufacturer's specifications using Dharmafect 1. After 8 h, C2C12 cells were exposed to low serum media (containing 2% horse serum) for the indicated times. When transfected alone, each siRNA led to significant GRAF1 depletion (and reduced induction of MHC), but combined treatment with 75 nM each led to a more pronounced reduction (data not shown) and was used in the data sets shown in Fig. 3.

Immunocytochemistry—Immunofluorescent staining of 4% paraformaldehyde-fixed cells was performed by standard procedures. Cells were incubated with primary antibodies at a 1:1000 dilution or with Texas Red phalloidin (1:1000) to visualize filamentous actin for 1 h at room temperature followed by 1 h of incubation with appropriate fluorescent secondary antibody.

Western Blotting—Embryos (n = 5–10) were snap-frozen in liquid nitrogen, and protein lysates were generated by brief (1–2 s) sonication in a modified RIPA buffer (10 mM Tris, pH 7.5, 100 mM NaCl, 1 mM EDTA, 1 mM EGTA, 20 mM $Na_4P_2O_7$, 1% Triton X-100 plus a mixture of protease and phosphatase inhibitors, including 1 mM Na_3VO_4, 40 mM NaF, 10 mM Na_2 pyrophosphate, 100 μM leupeptin, 1 mM 4-(2-aminoethyl)benzenesulfonyl fluoride hydrochloride, 0.02 mg/ml soybean trypsin inhibitor, and 0.05 trypsin inhibitory units/ml aprotinin). C2C12 or L6 cells were lysed directly in the RIPA buffer containing inhibitors. Fifty micrograms of clarified protein lysate was separated by SDS-PAGE, transferred onto nitrocellulose, and processed for Western analysis by standard procedures. In brief, following transfer to nitrocellulose, membranes were blocked in 5% dry milk in Tris-buffered saline (TBS) + 0.1% Tween (TBST) and incubated overnight with primary antibody diluted (1:1000) in blocking solution. Blots were incubated with the appropriate horseradish peroxidase-conjugated secondary antibodies (1:2000 dilution) (GE Healthcare), and proteins were visualized by chemiluminescence (Thermo Scientific).

RT-PCR Analysis—RNA was isolated from 10 embryos following lysis in TRIzol according to the manufacturer's specifications (Invitrogen). Reverse transcription reactions were performed using the iScript cDNA kit (Bio-Rad), and PCRs were performed using ExTaq polymerase (Takara Bio). RT-PCRs were performed using previously published primer sets and cycling parameters for *x-mhc* and *x-myogenin* (22, 23). Primers for histone H4 and *x-GRAF1* were forward 5′ GGG ATA ACA TTC AGG GTA TC 3′ and reverse 5′ CAT GGC GGT AAC TGT CTT C 3′ and *x-GRAF1* forward 5′-GCC AGG AGT CAA GAA TCA AGG 3′ and *x-GRAF1* reverse 5′ CAA CTC CAA GGT TGG CTA CAG TC 3′.

RhoA Activity Assays—One confluent 35-mm dish of L6 or C2C12 cells/time point or 10 embryos for each treatment (Con Mo- and GRAF1 Mo-injected) were collected at stage 22, and

tails were snap-frozen in liquid nitrogen for use in the G-LISA luminescence-based RhoA-specific activation assay (BK121, Cytoskeleton). 10 *Xenopus* tails/time point or one 35-mm dish of L6 or C2C12 cells were thawed on ice and immediately lysed in 100 μl of ice-cold lysis buffer containing protease inhibitors (supplied by the manufacturer) by sonication (1-s pulses at 20% power three times; Sonics VibraCell). Lysates were clarified by centrifugation (3 min at 4 °C), and RhoA activity was assessed with a final concentration of 1 mg/ml lysates as per the manufacturer's instructions (Cytoskeleton).

Cdc42 Activity Assays—GST-Pak (amino acid 1–290 of Pak1) was purified from bacterial lysates using glutathione-agarose beads as described previously (24). In brief, vector or GRAF1-transfected L6 myoblasts were lysed in Buffer A (50 mM Tris, pH 7.6, 500 mM NaCl, 0.1% SDS, 0.5% deoxycholate, 1% Triton X-100, 0.5 mM $MgCl_2$, plus 100 μM leupeptin, 1 mM 4-(2-aminoethyl)benzenesulfonyl fluoride hydrochloride, and 0.05 trypsin inhibitory units/ml aprotinin) and cleared by centrifugation for 10 min at 14,000 rpm at 4 °C. 500 μg of lysate was combined with 30 μg of GST-PAK, and samples were rotated at 4 °C for 30 min. The complexes were pelleted by centrifugation and washed three times in Buffer B (50 mM Tris, pH 7.6, 150 mM NaCl, 1% Triton X-100, 0.5 mM $MgCl_2$, plus 100 μM leupeptin, 1 mM 4-(2-aminoethyl)benzenesulfonyl fluoride, and 0.05 trypsin inhibitory units/ml). Samples were boiled in SDS-PAGE buffer, electrophoresed (15% SDS-polyacrylamide gel), and transferred to polyvinylidene difluoride (Bio-Rad). Western blotting was performed using an anti-Cdc42 primary antibody (Santa Cruz Biotechnology).

Statistical Analysis—Enzymatic assays were measured in triplicate, and statistical analyses were performed by paired two-tail *t* test. Data are expressed as mean ± S.E. and were considered statistically significant at $p < 0.05$. All Western blots were performed at least three separate times, and representative images are shown. Cellular phenotypes were scored from at least three separate experiments, and data were tabulated from a minimum of 150 cells per treatment group.

RESULTS

GRAF1 Is Expressed in Differentiating Myoblasts—Given our previous findings that GRAF1 was most abundantly expressed in terminally differentiated cells of adult mammalian tissues (heart and brain) (12, 13), we predicted that GRAF1-dependent inhibition of RhoA might play an important role in promoting cellular differentiation. Interestingly, we recently found that GRAF1 is transiently expressed at high levels in late embryonic/early neonatal rodent soleus muscle with peak expression occurring at post-natal day 4 (P4) when mammalian myoblasts undergo cell cycle withdrawal, differentiation, and fusion to form multinucleated myotubes (Fig. 1*A*) (25). Coupled with recent findings that down-regulation of RhoA is critical for myoblast differentiation, we sought to gain further insight into the relevance of GRAF1 expression during this dynamic process. C2C12 and L6 are well established multipotent mesenchymal progenitor cell lines that undergo spontaneous differentiation into multinucleated skeletal muscle myotubes when cultured under high confluence in low serum media (LSM) (26, 27). Western analysis revealed that GRAF1 expression was

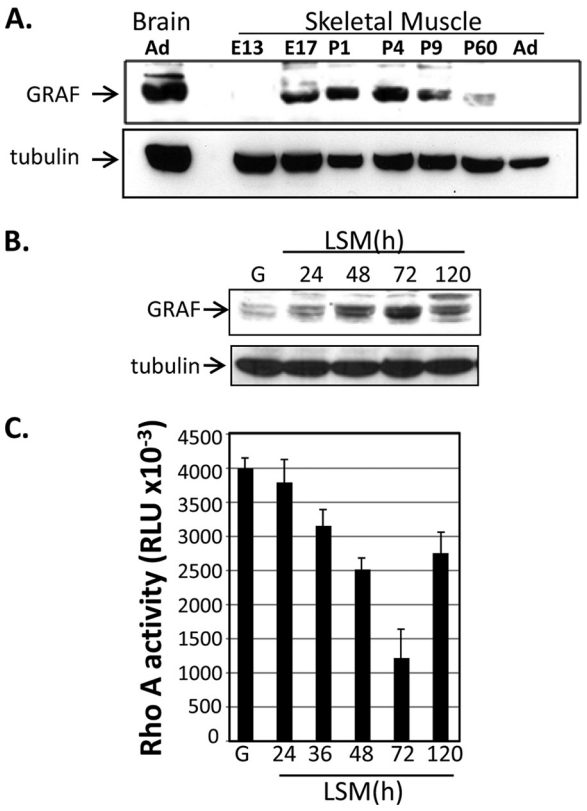

FIGURE 1. **GRAF1 expression is induced in differentiating myoblasts.** *A,* Western blot analysis of GRAF1 protein levels in embryonic (*E*), postnatal (*P*), and adult (*Ad*) rat hind-limb muscle or brain at the indicated time of development. *B,* C2C12 cells maintained in growth (*G*) media or exposed to differentiation conditions (LSM) for the indicated times were lysed, and cell extracts were immunoblotted with GRAF1 and tubulin-specific antibodies. *C,* C2C12 cells were treated as described in *B,* and lysates were subjected to an ELISA-based RhoA activity assay. Data are expressed as average relative light units (*RLU*) per time point ($n = 3$).

markedly induced upon subjecting C2C12 cells to differentiating conditions (Fig. 1*B*) and that GRAF expression was inversely correlated to RhoA activity (Fig. 1*C*). Interestingly, immunofluorescent staining revealed that GRAF1 was induced in a subset of C2C12 cells following exposure to LSM, and dual labeling with skeletal muscle differentiation markers myogenin, tropomyosin (Tm), or myosin heavy chain (MHC) revealed that GRAF1 expression was induced several hours before these differentiation markers (Fig. 2). Similar results were found in L6 myoblasts, although these cells expressed lower levels of the differentiation marker genes (data not shown).

GRAF1 Is Necessary for Myoblast Differentiation—We generated siRNAs specific to GRAF1 and transfected these siRNAs into proliferating C2C12 myoblasts to determine the role of GRAF1 in myogenic differentiation. Importantly, transfection with GRAF1 siRNAs led to a marked decrease in GRAF1 protein levels, and GRAF1-depleted C2C12 cells expressed significantly lower levels of myogenin, Tm, and MHC upon exposure to LSM (Fig. 3*A*). As well, GRAF1-depleted cells exhibited significantly higher levels of RhoA activity in comparison with control siRNA-treated cells (Fig. 3*B*). Importantly, treatment with Y27632 at the onset of LSM treatment completely restored MHC expression in GRAF-depleted myoblasts (Fig. 3*C*). Collectively, these data indicate that GRAF1 promotes skeletal muscle differentiation by limiting RhoA/ROCK signaling.

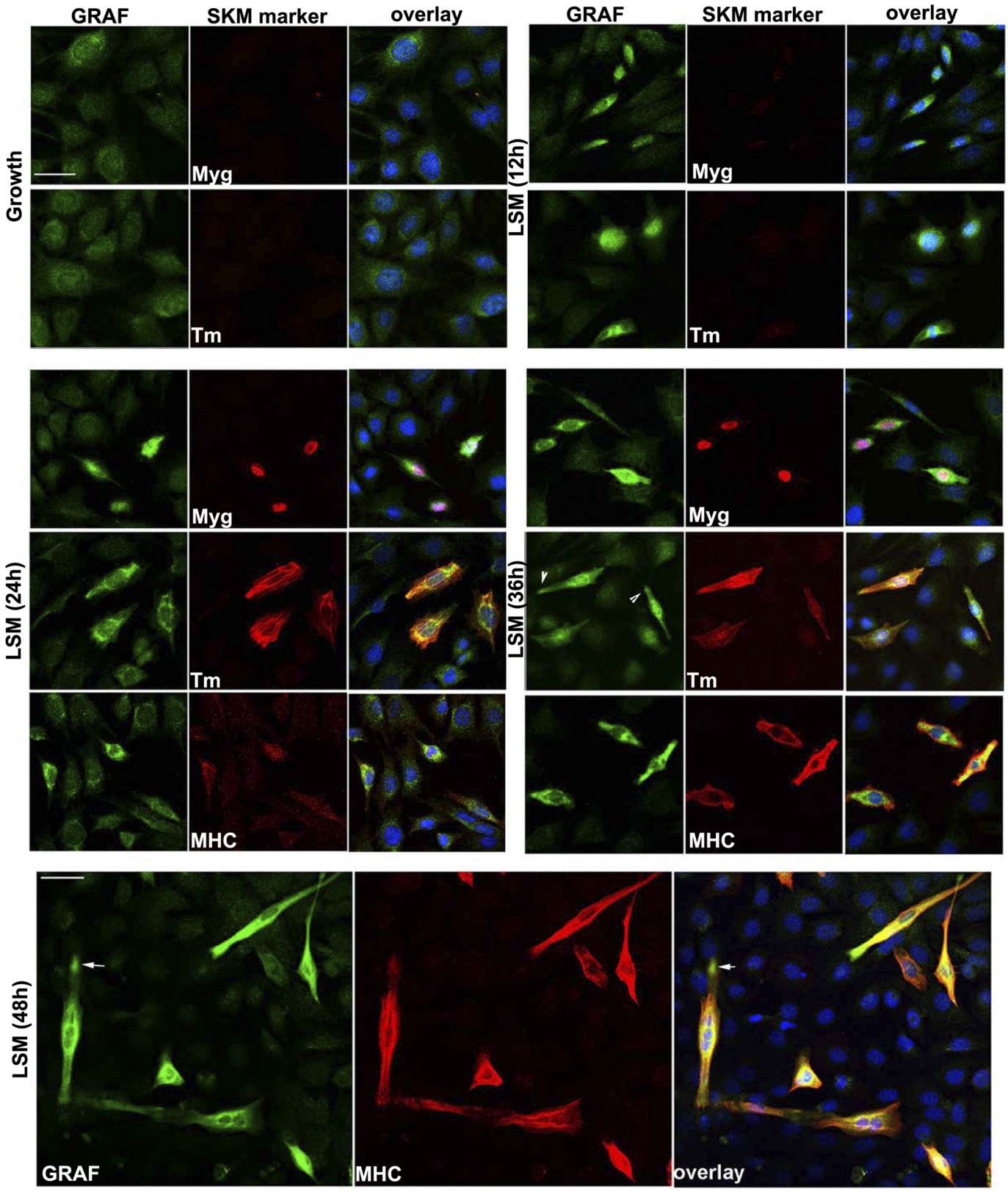

FIGURE 2. **GRAF1 up-regulation precedes expression of skeletal differentiation markers.** C2C12 cells maintained in growth (*G*) media or exposed to LSM for the indicated times were fixed and stained with GRAF1 (*green*) and indicated skeletal muscle differentiation marker (*red*; *Myg* (myogenin); *Tm* (tropomyosin); *MHC* (myosin heavy chain)). Nuclei were labeled with DAPI (*blue*). *Scale bar,* 50 μm. *Arrowheads* highlight GRAF recruitment to bi-polar tips of differentiated myoblasts (also see Fig. 7*A*).

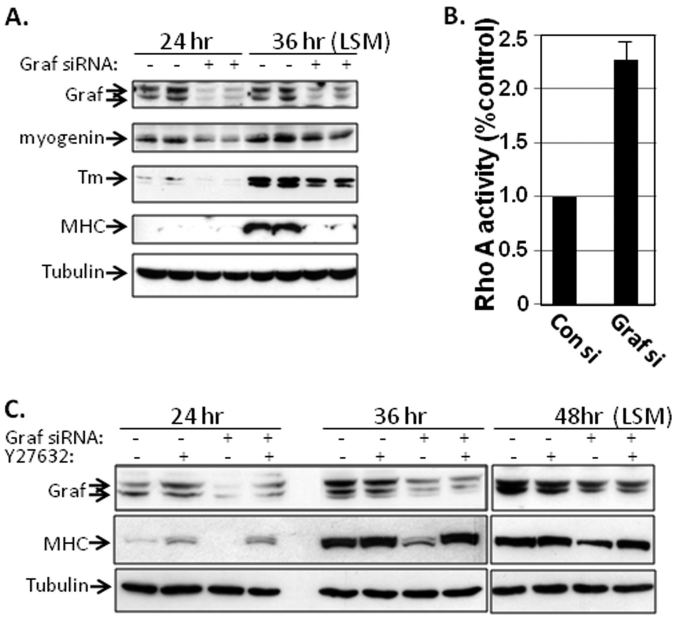

FIGURE 3. **GRAF depletion attenuates myoblast differentiation by increasing Rho/ROCK activity.** *A,* C2C12 cells were transfected with control or a mixture of two GRAF1-specific siRNAs, exposed to LSM for the indicated times, and cell extracts were immunoblotted with indicated antibody. Tubulin is shown as a loading control. Data are representative of three separate experiments. *B,* C2C12 cells were transfected with control or GRAF1-specific siRNAs and exposed to LSM for 72 h, and RhoA activity was measured an ELISA-based RhoA activity assay. Data represent the mean ± S.D. for three separate experiments. *C,* C2C12 cells were transfected with control or a mixture of two GRAF1-specific siRNAs, exposed to LSM with or without the ROCK inhibitor, Y27632 (10 μM), for the indicated times, and cell extracts were immunoblotted with indicated antibody. Tubulin is shown as a loading control. Data are representative of three separate experiments.

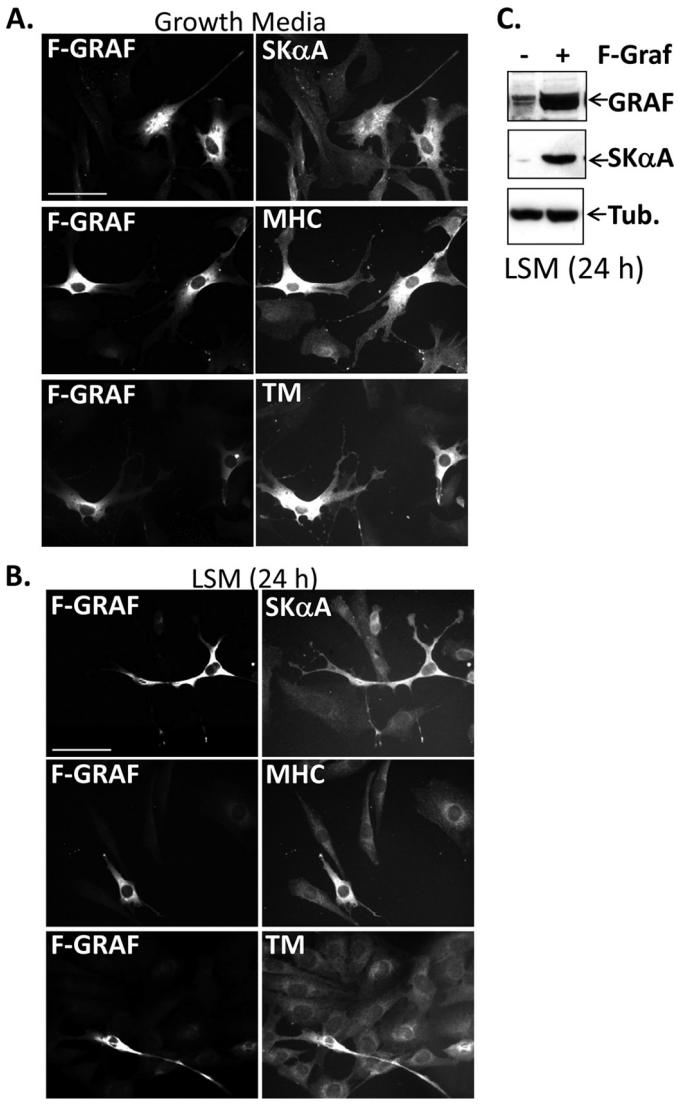

FIGURE 4. **GRAF promotes skeletal muscle differentiation.** *A* and *B,* C2C12 cells were transfected with FLAG GRAF (*F-GRAF*) and exposed to either growth media (*A*) or LSM (*B*) for the indicated times. Cells were stained with anti-FLAG antibody and co-stained with phalloidin and/or the indicated myogenic differentiation marker. $n = 250–350$ cells from 3–5 experiments. *Scale bar,* 50 μm. *C,* immunoblots of L6 cells transfected with vector control (−) or F-GRAF and exposed to LSM for 24 h. *Tub,* tubulin.

GRAF1 Promotes Skeletal Muscle Differentiation in a GAP-dependent Fashion—Because high levels of Rho activity may be critical for maintaining C2C12 cells in an immature and proliferative state under growth conditions, we next examined whether ectopic expression of GRAF1 might be sufficient to promote skeletal muscle marker expression in these cells by inactivating Rho. Indeed, we found that expression of wild type FLAG-GRAF1 markedly induced skeletal muscle differentiation marker expression in C2C12 and L6 cells cultured in either growth media or LSM as assessed by immunohistochemistry for skeletal α-actin (SKA), MHC, or Tm (Fig. 4, *A* and *B*) and Western analysis for SKA (Fig. 4*C*). GRAF1-transfected cells also appeared elongated and spindle shaped, the morphological features of differentiated myoblasts (7).

To determine whether GAP activity was necessary for GRAF1-dependent induction of differentiation, we expressed a GRAF1 variant containing a point mutation in the GAP domain (R412Q) that blocks enzymatic activity (12). Importantly, transfection with GRAF1 (but not ^{R412Q}GRAF1; hereafter referred to as GAPm; Fig. 5*A*) markedly attenuated RhoA (but not Cdc42) activity in cultured L6 cells (supplemental Fig. S1, *A* and *B*). As expected, transfection with the GAP-deficient variant (GAPm) failed to induce skeletal muscle differentiation marker gene expression of C2C12 cells cultured in growth (data not shown) or LSM (Fig. 5, *B* and *D*). Interestingly, ectopic expression of the GAP domain alone conferred only partial activity, indicating that additional functional domains of GRAF1 are required for its ability to promote myoblast differentiation (Fig. 5*D*). In support of this idea, we found that a GRAF1 variant engineered with a mutation to a conserved tryptophan residue in the SH3 domain (E719Q; referred to as SH3m), which we previously showed was required for the ability of GRAF1 to bind FAK and to translocate to focal adhesions, had a significantly decreased ability to induce differentiation (assessed by tropomyosin expression) when compared with wtGRAF1 (Fig. 5*D*). These data indicate that both GAP activity and SH3-mediated protein interactions are required for the optimal induction of the skeletal differentiation program.

Interestingly, GRAF1 but not GAPm induced terminal differentiation of C2C12 cells grown in LSM as determined by marked induction of the cyclin-dependent kinase inhibitor, p21 (a marker of irreversible arrest (28)), and precocious promotion of multinucleation (Fig. 5*C*). Indeed, all GRAF1-expressing

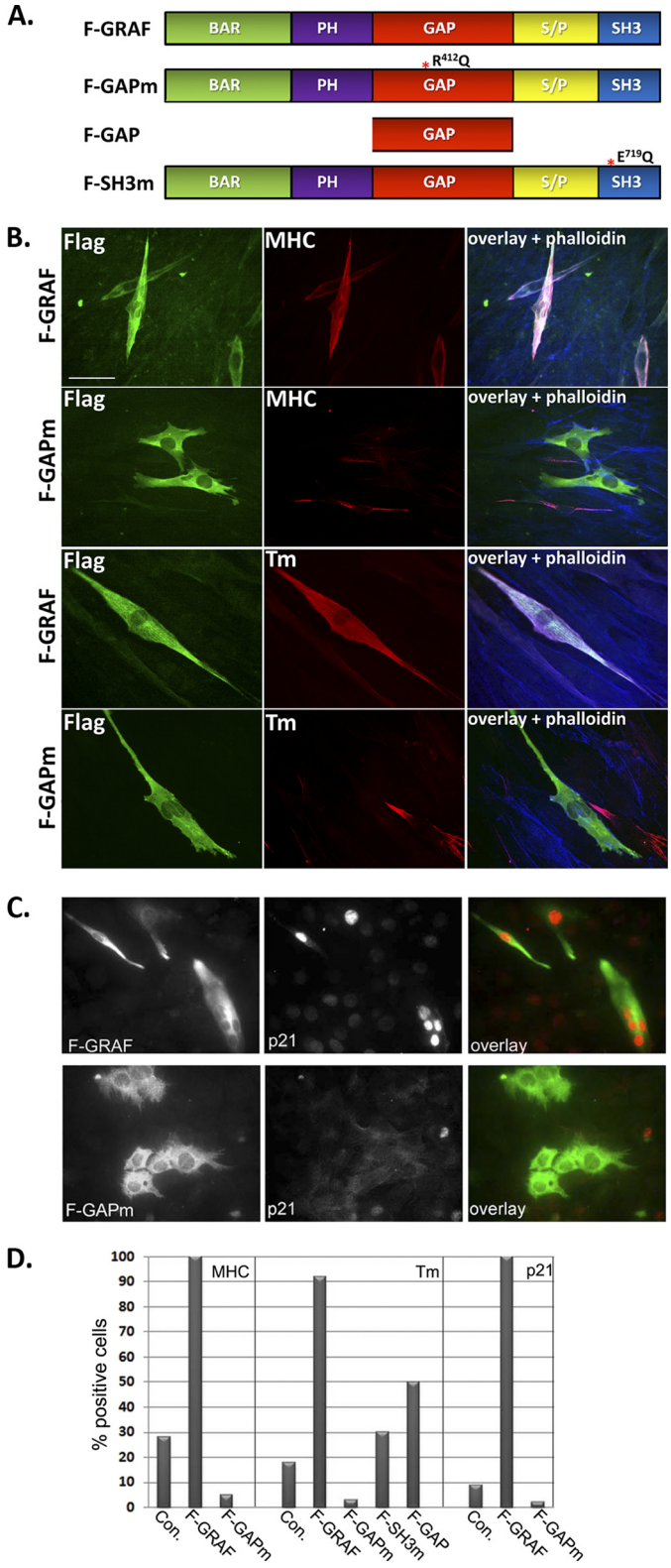

FIGURE 5. **GRAF promotes terminal differentiation of myoblasts in a GAP- and SH3-dependent fashion.** *A,* schematic showing full-length FLAG-tagged GRAF (*F-GRAF*) and GRAF variants used herein. *PH*, pleckstrin homology; *S/P*, serine/proline-rich domain. *B* and *C,* C2C12 cells were transfected with FLAG GRAF1 (*F-GRAF*) or FLAG GRAF1^{R412Q} (*F-GAPm*) and exposed to LSM for 48 (*B*) or 72 h (*C*). Cells were stained with anti-FLAG antibody to detect GRAF variants (*green*) and co-stained with phalloidin and tropomyosin (*Tm*) or p21^{cip}. *Scale bars,* 50 μm. *D,* quantification of GRAF-induced skeletal differentiation marker gene expression. The number of cells positive for the indicated marker was counted in control (*Con*) and GRAF (or indicated GRAF variant-)-expressing cells exposed to LSM for 48 h. Data represent the % of expressing cells counted in three to five separate experiments (n = 200–350 cells/condition).

cells were p21-positive following a 72-h treatment with LSM, whereas only 12% of vector-treated cells expressed p21 at this time point. Moreover, nearly 30% of GRAF1-expressing cells were multinucleated by day 3 of differentiation, whereas nearly all vector or GAPm-transfected controls remained unfused (less than 2% were multinucleated). Taken together, these data demonstrate that expression of GRAF1 promotes cell cycle withdrawal and terminal differentiation in a Rho-GAP-dependent fashion.

GRAF1 Promotes Myoblast Fusion—Cell fusion occurs between muscle cells that have undergone early differentiation events (*i.e.* expression of contractile proteins), and therefore GRAF1-dependent enhancement of differentiation alone could lead to enhanced myotube formation. Thus, to determine whether GRAF1 can directly impact myotube fusion in pre-differentiated cells, we expressed Cre-inducible GRAF1 cDNA variants (hereafter referred to as GRAF1^{loxp} or GAPm^{loxp}; Fig. 6*A*) to enable time-dependent induction of GRAF1 expression. Transient transfection of GRAF1^{loxp} and GAPm^{loxp} led to GFP but not GRAF1 expression in cells treated with LacZ control virus, but GRAF1 expression was markedly induced in parallel cultures treated for 24 h with Cre adenovirus (Fig. 6*B*).

To assess a specific role for GRAF1 in promoting fusion of differentiated myoblasts, cells were transfected with GRAF1^{loxp}, transferred to differentiation media for 4 days, and then treated with Cre or LacZ adenoviruses. As shown in Fig. 6, *C–E*, GRAF1-expressing L6 cells (in the Cre-treated cultures) exhibited a marked increase in myotube fusion in comparison with nontransfected controls. Although control (LacZ-treated) transfectants contained up to three nuclei per cell, nearly two-thirds of GRAF1-expressing cells contained greater than 30 nuclei. Furthermore, the majority of Cre-treated GAPm-expressing cells (like the Lac Z controls) contained only 1–3 nuclei (Fig. 6, *D, bottom,* and *E*). Similar findings were observed upon GRAF1 expression in pre-differentiated C2C12 cells (see Fig. 6, *C* and *D*). These data confirm that GRAF1 expression can promote fusion of differentiated myoblasts in a GAP-dependent manner.

GRAF1 Regulates Actin Organization in Pre-fused Myoblasts—Although a complete understanding of the mechanisms governing skeletal muscle fusion is lacking, it is clear that dramatic reorganization of the cytoskeleton occurs during this dynamic process (7). In particular, previous studies have revealed that the formation and subsequent dissolution of an F-actin focus at the distal ends of fusion-competent myoblasts are essential for myoblast-myoblast fusion (8). To determine whether GRAF1 might play an important role in cytoskeletal remodeling that accompanies myoblast fusion, we first examined the subcellular localization of endogenous GRAF1 in pre-fused myoblasts. Endogenous GRAF1 localizes to leading edge lamellipodia and dorsal ruffles as well as a cytoplasmic perinuclear compartment in myoblasts maintained in growth media (Fig. 2, *top left,* and supplemental Fig. S2*A*). Co-staining with SKA and high power image merging revealed only a partial overlap between the two

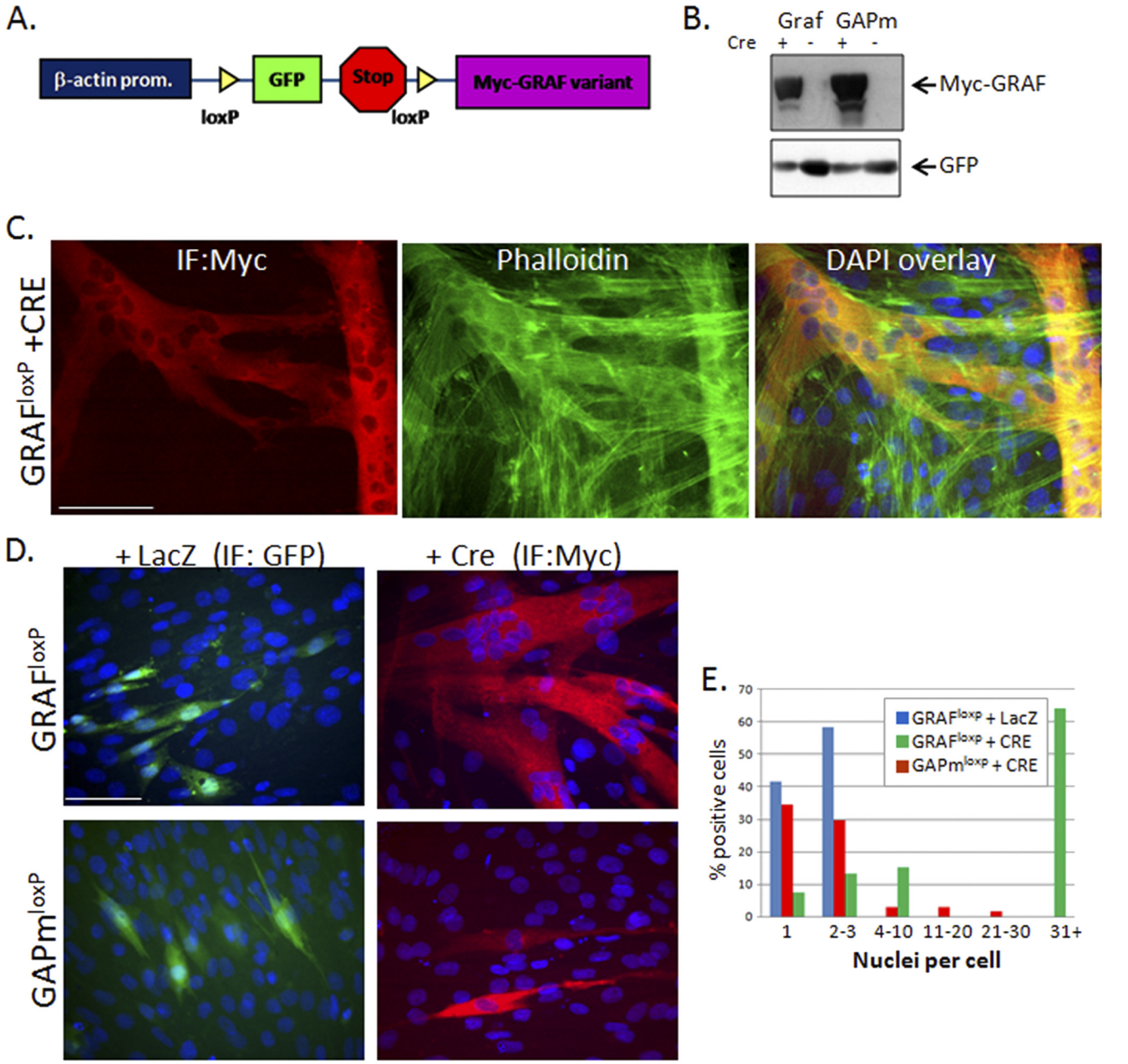

FIGURE 6. **GRAF1 promotes fusion of pre-differentiated myoblasts.** *A,* schematic of Cre-inducible Myc-tagged GRAF1 targeting constructs (denoted GRAF1^{loxp} and GAPm^{loxp}). *B,* COS cells were transfected with GRAF1^{loxp} or GAPm^{loxp} targeting constructs and treated with Cre (+) or control, LacZ (−) adenovirus for 24 h. Cells were lysed and immunoblotted with the indicated antibodies. *C–E,* L6 myoblasts were transfected with GRAF1^{loxp} or GAPm^{loxp}, exposed to LSM for 4 days to induce differentiation, and transduced with LacZ or Cre adenovirus for 48 h. Dual Myc and DAPI staining revealed marked cell fusion in GRAF1 (but not GAPm)-expressing cells in comparison with controls. Quantification of cell numbers from three independent experiments is shown graphically (*E, n* = 150–250 cells). *IF,* immunofluorescence. *Scale bar,* 50 μm.

proteins, wherein GRAF1 was predominantly localized to the innermost face of these actin-based structures (supplemental Fig. S2*A*). Upon shifting cells to LSM, GRAF1 redistributes to the bi-polar tips of elongating myoblasts (Fig. 2, *middle* and *bottom panels,* and Fig. 7*A*). As well, co-staining with phalloidin and tropomyosin indicates that these regions are nearly completely devoid of actin-based structures (Fig. 7*A*, *right*).

We reasoned that GRAF1 localization to these discrete sites may be important for limiting the extent of Rho-dependent F-actin polymerization. To address this question, we ectopically expressed F-GRAF1 or GAPm in subconfluent myoblasts and co-stained with phalloidin to detect filamentous actin. F-GRAF1 but not GAPm induced marked clearing of actin stress fibers in myoblasts maintained in serum-containing media (Fig. 7*B*). As well, the width of polymerized actin foci was narrower in GRAF1-expressing cells cultured in LSM than in nontransfected cells or cells expressing GAPm (Fig. 7, *C* and *D*). Moreover, significant overlay between GAPm and polymerized actin was observed through the entire width of the actin focus, although the F-GRAF1-labeled region was mostly devoid of polymerized actin (Fig. 7*C, overlay, right panel*). From these data, we surmise that GRAF1 recruitment to the tips of differentiating myoblasts reduces subplasmalemmal actin polymerization resulting in the dissolution of actin foci and the elonga-

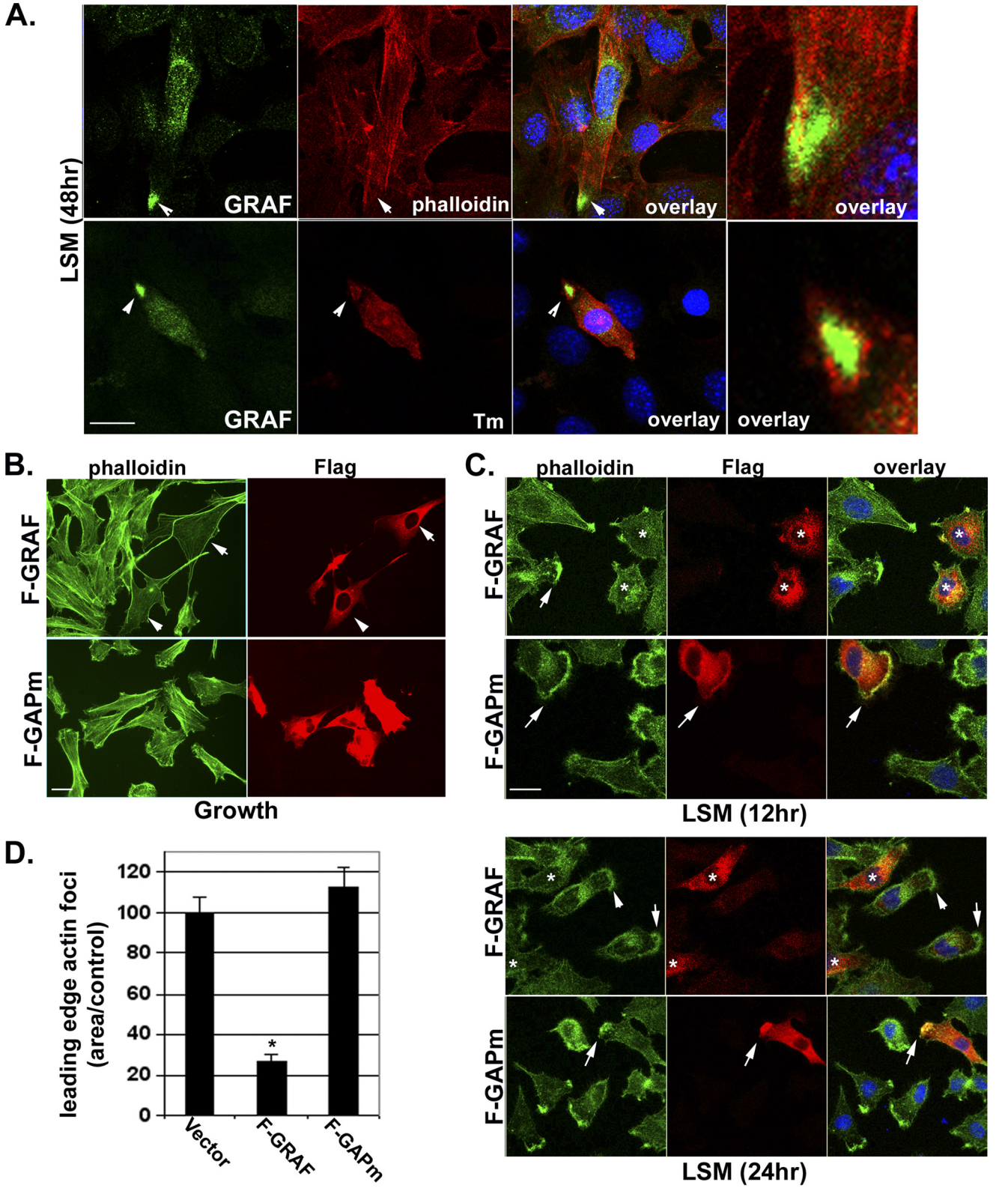

FIGURE 7. **GRAF1 is recruited to a pre-fusion complex and promotes actin-foci dissolution.** *A*, C2C12 cells were exposed to differentiation conditions (LSM) for 48 h, and endogenous GRAF1 was detected by confocal immunofluorescence microscopy. Note high level of GRAF1 protein localized to the tips of pre-fused myoblasts. Co-staining with phalloidin to detect filamentous actin or Tm reveals lack of actin-based structures in the GRAF localization domain (*arrowheads*). *Scale bar*, 50 μm. *B* and *C*, L6 myoblasts transfected with F-GRAF or F-GAPm in growth media or LSM for the indicated time points. Cells were co-stained with anti-FLAG antibody and phalloidin. Overlay shows high magnification merge of GRAF1 variants and phalloidin. *Scale bars*, 50 μm. *D*, quantification of areas of actin foci at the leading edge of F-GRAF and F-GAPm cells is shown graphically (n = at least 100 cells/condition from 3 experiments). *, $p < 0.05$.

tion of pre-fused myoblasts. In support of this theory, prolonged expression of GRAF1 in subconfluent myoblasts maintained in growth medium leads to continuous growth of actin-based filopodial extensions (supplemental Fig. S2*B*), possibly due, at least in part, to un-checked activity of Rac- and Cdc42, as was previously observed in GRAF1-expressing fibroblasts (12).

GRAF1-dependent Myotube Formation Requires BAR-mediated Membrane Binding or Sculpting—In addition to the GAP and SH3 domains, GRAF1 contains a BAR domain that functions to bind and deform plasma membranes and to regulate endocytosis (29, 30). Because endocytic recycling/trafficking has been implicated in the merging of membrane bilayers from two apposing cells during myotube formation (31–34, we reasoned that this domain might also play a critical role in GRAF1-dependent myoblast fusion. To test this hypothesis, we generated two GRAF1 variants that either lacked the first 280 amino acids of GRAF1 that comprise the BAR domain (referred to as ΔBAR) or that contained mutations in key lysine residues in the BAR domain (K121E/K131E/K132E) shown previously to render the protein incapable of lipid bending (referred to as BARm; see Fig. 8*A*) (29). Both GRAF1 BAR variants (like wtGRAF1) induced marked expression of Tm in cells exposed to LSM for 24 h, indicating that the BAR domain is not necessary for mediating GRAF1-dependent myoblast differentiation (Fig. 8*B*). Although the BAR mutants appropriately localized to the bipolar tips of differentiated myoblasts (indicated by *arrows* in Fig. 8*C*), the induction of multinucleated myotubes observed at 72 h was dramatically reduced in ΔBAR- and BARm-expressing cells (less than 2%) compared with those expressing wild type GRAF1 (33%; Fig. 8*C*). A similar lack of myotube formation was observed when ΔBAR^{loxP} expression was induced in pre-differentiated C2C12 myoblasts, using the aforementioned Cre-dependent strategy, despite clear membrane association of this variant (Fig. 8, *D* and *E*).

GRAF1 BAR mutations have been associated with elevated GAP activity via relief of auto-inhibition induced by direct interaction between the BAR and GAP domains (30). Because previous studies revealed that blocking Rho activity (by expression of a dominant-interfering mutant, N19RhoA, or by inclusion of the Rho kinase inhibitor, Y27632) *enhanced* myoblast fusion (3), one might expect that if the BAR domain was not essential for myoblast fusion then BAR mutants would be even more effective at promoting fusion than wtGRAF1. Nonetheless, additional experiments were performed to ensure that the inability of GRAF1 BAR variants to induce intercellular fusion was not due to the elevated GAP activity associated with BAR mutations. To this end, we generated Cre-inducible constructs that express dominant-negative (N19) or constitutively active (L63) RhoA (supplemental Fig. S3*A*). Using the previously described experimental paradigm, we examined the ability of L63RhoA to induce fusion of pre-differentiated myoblasts when co-expressed with ΔBAR^{loxP}. We found that L63RhoA was incapable of rescuing myotube formation when expressed over a 30-fold range of concentrations (0.1–3:1 L63RhoA/ΔBAR, data not shown). We next evaluated whether additional down-regulation of Rho activity would impair wtGRAF1-dependent myotube formation. As was reported previously (3), we found that inactivation of Rho (by induced expression of N19RhoA or by treatment with Y27632) promoted fusion of pre-differentiated myoblasts (albeit to a lesser extent that wtGRAF1; supplemental Fig. S3*B*). Importantly, expression of N19RhoA or treatment with Y27632 did not impair (indeed slightly enhanced) the ability of wtGRAF1 to promote myotube formation (supplemental Fig. S3*C*). Thus, the lack of fusion in the BAR mutants was not secondary to elevated GAP activity (30). Collectively, these data indicate the following: 1) GRAF1 promotes robust myotube formation *in vitro*; 2) Rho-GAP activity is necessary to mediate GRAF1-dependent myoblast differentiation and fusion; and 3) fusion requires additional BAR-dependent membrane bending or sculpting.

GRAF1 Is Expressed during Xenopus Somite Development—We next strove to determine whether GRAF1 is a major regulator of Rho activity and muscle development *in vivo*. To this end, we explored the effect of GRAF1 depletion in developing *X. laevis* embryos using an antisense-morpholino approach. *Xenopus* GRAF1 contains each of the functional domains previously defined in chicken and mammalian GRAF1, including, in tandem, a BAR domain, pleckstrin homology domain, GAP domain, and SH3 domain and the overall amino acid identity of *Xenopus* GRAF1 protein to its orthologues in human and mouse are 83.8 and 77.5%, respectively (NCI-Blast), indicating that the function of this protein is likely evolutionarily conserved between these species.

Because *Xenopus* GRAF1 had not been previously studied, we first performed semi-quantitative RT-PCR analysis to characterize GRAF1 expression during development. As shown in Fig. 9*A*, *x.GRAF1* transcript is present at low levels throughout early development, and expression increases from stage 25 through tadpole stages. To assess the tissue distribution of GRAF1 in *Xenopus*, we performed a whole-mount *in situ* hybridization analysis of stage 29 embryos using a probe directed toward the 3′UTR of *x.GRAF1*. In accordance with our previous findings in rodents, we observed high levels of *x.GRAF1* expression in the heart and brain (Fig. 9*B*). *x.GRAF1* was also abundant in the eyes, neural tube, dorsal root ganglia, and somites (*i.e.* skeletal muscle precursors, note segmental pattern; Fig. 9, *B* and *C*). As shown in Fig. 9*D*, GRAF1 protein levels closely mirrored GRAF1 mRNA levels during *Xenopus* development with low levels during gastrulation that progressively increased between stages 22 and 37 (see supplemental Fig. S4 for antibody characterization). GRAF1 was further up-regulated (~3-fold) at stage 52, when intercellular fusion between myoblasts occurs (supplemental Fig. S5*A*). Although low levels of GRAF1 were apparent along the lateral edges of the myofibrils (particularly at early stages), GRAF1 protein was predominantly localized at the tips of the myofibers directly adjacent to the myoseptum in embryos from stage 25 (supplemental Fig. S5*B*) to 37 (Fig. 9*E*). This structure, akin to myotendinous junctions in mammals, is the major site of force transmission from myofibrils across the muscle cell membrane to the extracellular matrix and underlying skeleton.

GRAF1 Depletion Leads to Swimming Defects and Embryonic Lethality—Injection of GRAF1 morpholinos (GRAF1 Mo) that targeted sequences upstream of (denoted mo1) and flanking the

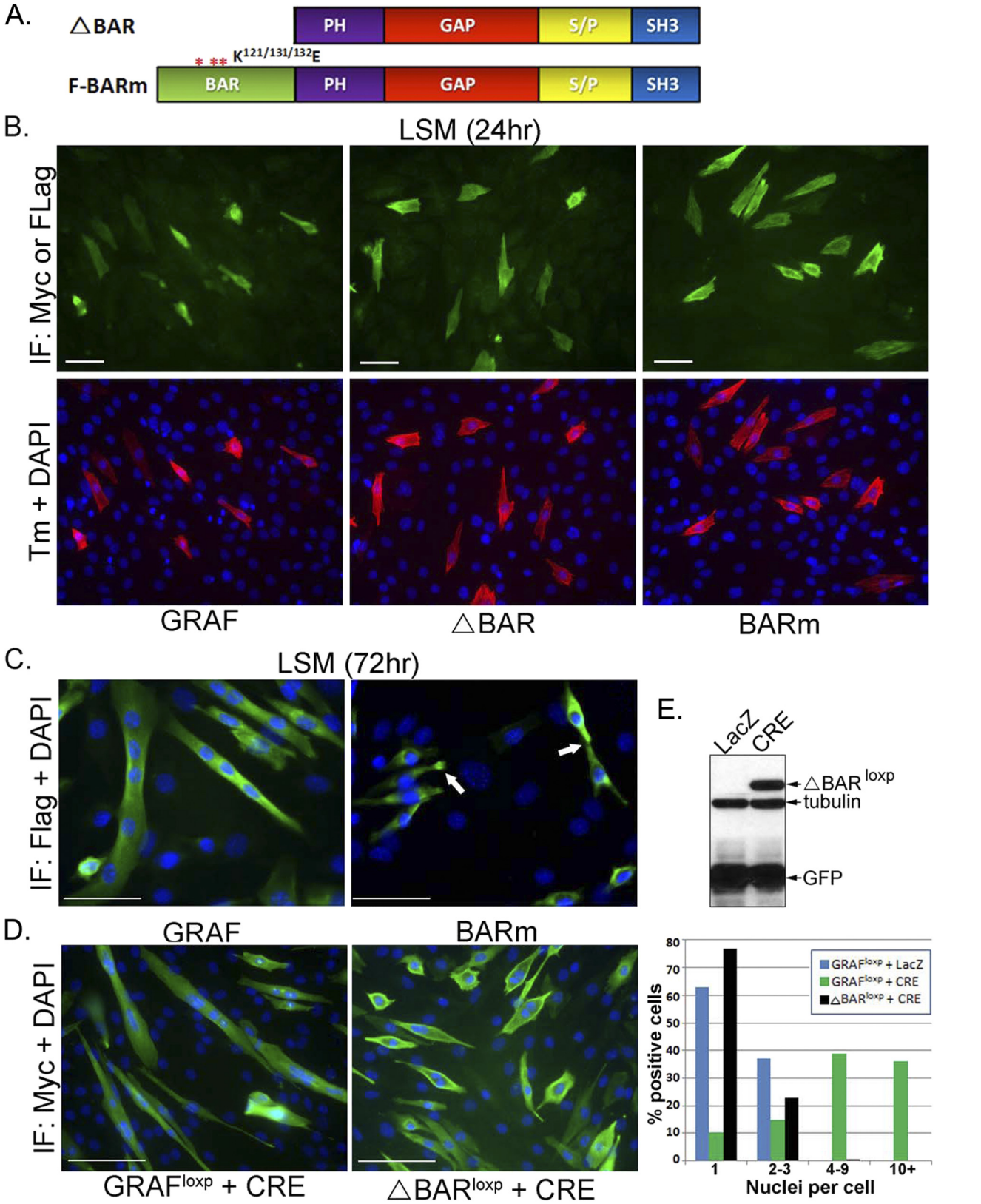

FIGURE 8. **GRAF1-dependent myotube fusion requires the BAR domain.** *A,* schematic of GRAF BAR variants. *PH*, pleckstrin homology; *S/P*, serine/proline-rich domain. *B* and *C,* C2C12 cells were transfected with F-GRAF, F-BARm, or F-ΔBAR variants, exposed to LSM for 24 or 72 h, and stained as described above. Tm (*red*), GRAF1 variant (*green*), and nuclei (*blue*). Greater than 95% of GRAF1 and GRAF1 BAR variant expressing cells co-expressed high levels of Tm (n = 150–200 cells from 3 experiments). *Arrows* denote appropriate recruitment of BARm to the plasma membrane and presumptive pre-fusion sites. *IF,* immunofluorescence. *D,* C2C12 myoblasts were transfected with GRAF1^{loxp} or ΔBAR^{loxp}, exposed to LSM for 4 days to induce differentiation, and transduced with LacZ or Cre adenovirus for 48 h. Quantification of cell numbers from three independent experiments is shown graphically (*right panel*; n = 200–250 cells). Separate experiments showed similar results after induction for up to 96 h (data not shown). *E,* COS cells were transfected with the ΔBAR^{loxp} targeting construct and treated with Cre or control, LacZ adenovirus for 24 h. Cells were lysed and immunoblotted with the indicated antibodies.

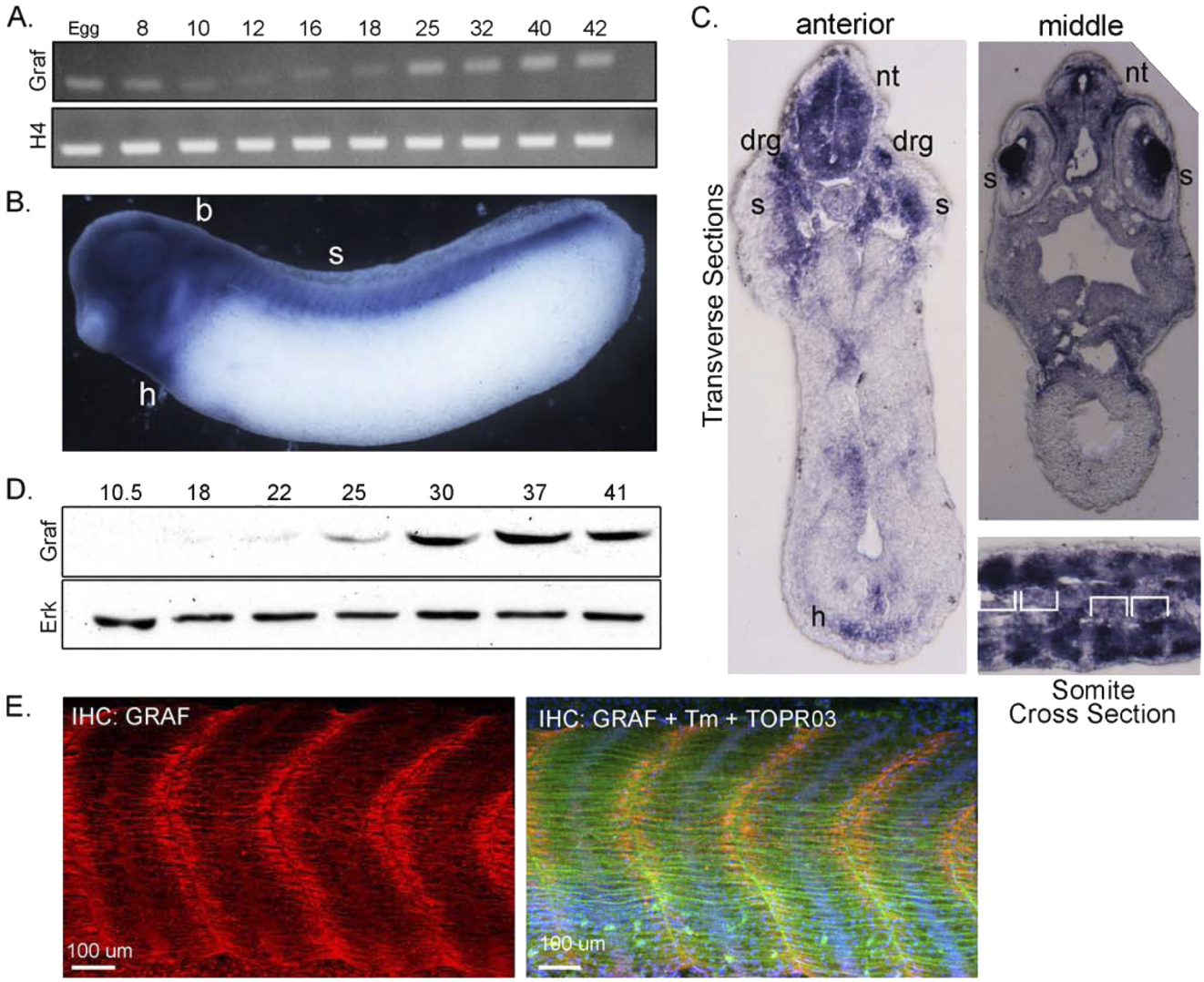

FIGURE 9. **GRAF1 is highly expressed during somitogenesis.** *A,* RT-PCR analysis for *x.GRAF1* and histone H4 (*H4*; loading control) was performed using RNA isolated from embryos at the indicated stages. *B* and *C,* whole-mount *in situ* hybridization of stage 29 *Xenopus* embryo using an antisense probe specific for *x.GRAF1*: *h,* heart; *b,* brain; *s,* somites; *nt*, neural tube; *drg*, dorsal root ganglia. *B,* lateral view. *C, top*, transverse; *bottom*; cross-section through mid-somite region (somite borders indicated with *brackets*). *D,* Western blot analysis of GRAF1 and ERK (loading control) expression at the indicated developmental stages. *E,* laser scanning confocal images of whole-mount GRAF1 (*red*), tropomyosin (*green*), and ToPro3 (*blue* nuclei) stained somites from wild type stage 37 embryo. *IHC*, immunohistochemistry.

start codon (denoted mo2) of *x.GRAF1* at the one-cell stage markedly reduced embryonic GRAF1 levels at all stages tested between stage 18 and 37 (Fig. 10*A*; see supplemental Fig. S6 for further morpholino characterization). Importantly, GRAF1 immunoreactivity at the myoseptal boundaries was markedly reduced in stage 37 GRAF1 morphants, further supporting the specificity of our GRAF1 antibody and our immunofluorescent methods (supplemental Fig. S6*C*). Gross morphological assessment of developing Con Mo- and GRAF1 Mo-injected embryos indicated that gastrulation and neurulation were unperturbed in the GRAF1 morphants (supplemental Fig. S7*A*). However, this finding does not exclude a role for GRAF1 in these processes because maternally derived GRAF1 protein (that is not affected by morpholino injection) is apparent in the GRAF1 morphant embryos through stage 11 (Fig. 10*A*). However, all GRAF1 morphant embryos died by the time Con Mo-injected sibling embryos reached stage 42. By stages 37–39, many GRAF1 morphant embryos exhibited edema and lateral bending, and some exhibited diminished anteroposterior axis extension (Fig 10*B* and supplemental Table S1). A small percentage of GRAF1 Mo-injected embryos (~2%) arrested during development as demonstrated by marked anteroposterior axis shortening and diminished eye pigmentation. These embryos were not utilized for later analyses.

The most readily observed phenotype in GRAF1 Mo-injected embryos was a fully penetrant and striking swimming defect (supplemental Table S1 and supplemental movies 1 and 2) that was apparent between stages 35 and 39 (even in embryos that were indistinguishable from controls at a gross morphological level). Specifically, whereas Con Mo-injected embryos swam normally in response to touch, GRAF1 morphant embryos were either completely unable to swim (49%) or exhibited very limited movement of the tail (51%). In addition, the spontaneous swimming behavior seen in control tadpoles was completely absent in GRAF1 morphant embryos suggesting that the defect was not a defect in touch response alone. Interestingly, the hearts of GRAF1-depleted

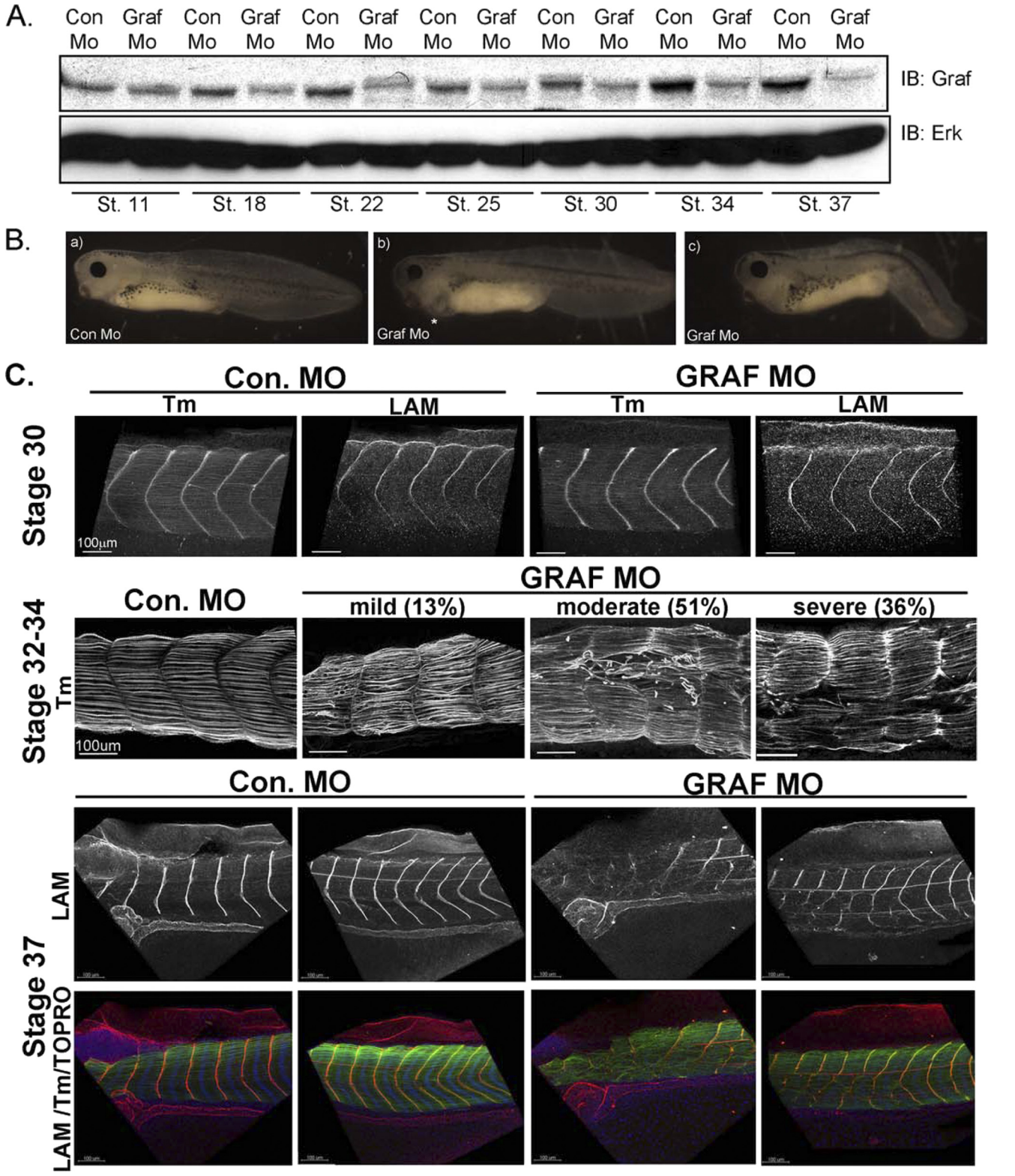

FIGURE 10. **GRAF1 is essential for maintaining somite architecture and myoseptal boundaries.** *A*, Western blot analysis for GRAF1 in Con MO- and GRAF1 Mo-injected embryos at the indicated stages of development. *IB*, immunoblot; *St.*, stain. *B*, stage 39 GRAF1 Mo-injected embryos exhibit edema (*panel b*) and anteroposterior axis defects (*panel c*) relative to control embryo (*panel a*). *C*, laser scanning confocal images of whole-mount stage 30–37 Con Mo- and GRAF1 Mo-injected somites reveal progressive degeneration. Embryos were stained with Tm or laminin (*LAM*) to visualize cells or myosepta, respectively.

embryos exhibited normal rhythmic contractions (data not shown), suggesting the presence of intact functional innervations. Importantly, injection of 5-bp mismatch morpholinos had no effect on GRAF1 protein levels or on *Xenopus* development (data not shown), indicating that these aforementioned phenotypes were due to GRAF1 depletion.

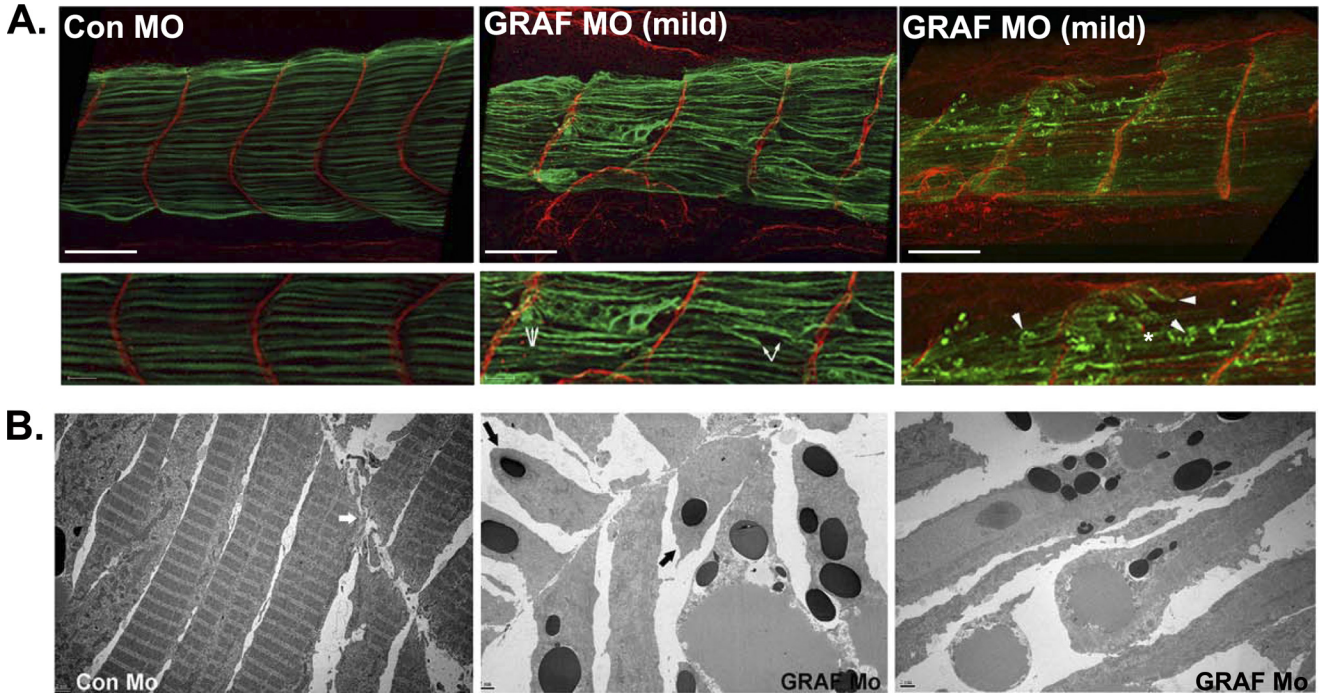

FIGURE 11. **GRAF1 depletion leads to fiber rupture.** *A,* laser scanning confocal microscopy of mildly affected stage 34 somites with Tm (*green*) and laminin (*LAM*) (*red*) reveal mid-somite tears (denoted by *arrows*). Laminin association with fiber tip is denoted by an *asterisk*. *Scale bar,* 100 μm. *B,* TEM (×2500 magnification) of somite-matched stage 37 Con Mo- and GRAF1 Mo-injected embryos. The myoseptum is denoted by a *thick white arrow* in the *Con Mo panel*. The sarcolemma remained attached to the intersomitic boundary in GRAF1 morphants, but mid-myofiber tears were prevalent (*black arrows*).

Xenopus GRAF1 Is Necessary for Maintaining Skeletal Muscle Integrity—Laser scanning confocal microscopic analysis of whole-mount Tm- and laminin-stained stage 30–37 control and GRAF1 morphant embryos revealed that GRAF1 is necessary for maintaining somite architecture (Fig. 10*C*). At stage 30, the organization of Tm-positive cells and the levels and continuity of laminin at repetitive intersomitic boundary units were comparable between control and GRAF1 morpholino-injected embryos (Fig. 10*C*). However, between stages 32 and 34, all GRAF1 morphants evaluated exhibited muscle fiber degeneration, and most (87%) had accompanying defects in somite boundaries. The embryos were categorized as having a mild, moderate, or severe phenotype using the following scheme: mild (13%), myofiber splitting or detachment with maintenance of somite boundaries; moderate (51%), myofiber splitting or detachment accompanied by loss of myoseptal integrity in up to 30% of the somites; severe (36%), myofiber splitting or detachment accompanied by disruption of 30% or more somite boundaries per embryo. Although examples of severe disruptions were found in the all regions of stage 34–37 GRAF1 morphant embryos, the middle region was most severely affected. By stage 37, all (33/33) GRAF1 morphant embryos evaluated exhibited markedly disrupted myoseptal segmentation (as demonstrated by the mosaic pattern of laminin staining) likely due to repair of earlier muscle tears. Collectively, these findings indicate that GRAF1 depletion leads to progressive somite degeneration.

To better understand the pathogenesis of muscle deterioration in the GRAF1 morphants, we closely evaluated the somites of stage 32–34 embryos that exhibited mild or moderate phenotypes. As shown in Fig. 11*A*, these phenotypes were associated with mid-somite cellular lesions accompanied by retraction of the cell body (demarcated by Tm, *green*). Interestingly, the tips of most cells appeared to remain in contact with the intersomitic boundary (Fig. 11*A*, demarcated by *LAM*, *red*). Indeed, ultrastructural analysis by TEM confirmed that the attachment of the sarcolemma to the intersomitic boundary was often maintained in GRAF1 morphants (Fig. 11*B*, *middle panel*), indicating that GRAF1 is not necessary for maintaining adhesion of the muscle fibers to the extracellular matrix-based myoseptum. However, mid-somite sarcomeric degeneration was evident (Fig. 11*B*, *right panel*) as was complete severing through terminal sarcomeric units (Fig. 11*B, middle panel, black arrows*). In addition, some cells appeared to have dissociated from the myosepta with laminin bound to the detached cell tips (denoted by *asterisk* in Fig. 11*A, right panel*) indicating that there may be additional defects in matrix assembly/maintenance.

GRAF1 Depletion Does Not Disrupt Somite Specification, Somite Rotation, or Boundary Formation—In an effort to define the precise GRAF1-dependent step(s) that lead to myofiber and myoseptal degeneration, we first assessed whether GRAF1 depletion altered the early specification of the somites. To this end, we performed whole-mount *in situ* hybridization analysis of MyoD that is expressed in a segmental pattern in the presomitic mesoderm of *Xenopus* from the neurula onward. No differences in the spatial distribution of MyoD RNA were observed between Con or GRAF1 MO-injected embryos analyzed from stages 18 to 34 (stages 24–34 shown in supplemental Fig. S7*B*), suggesting that somites were properly specified in the absence of GRAF1. In accordance with our *in situ* analysis, no significant differences in the levels of MyoD tran-

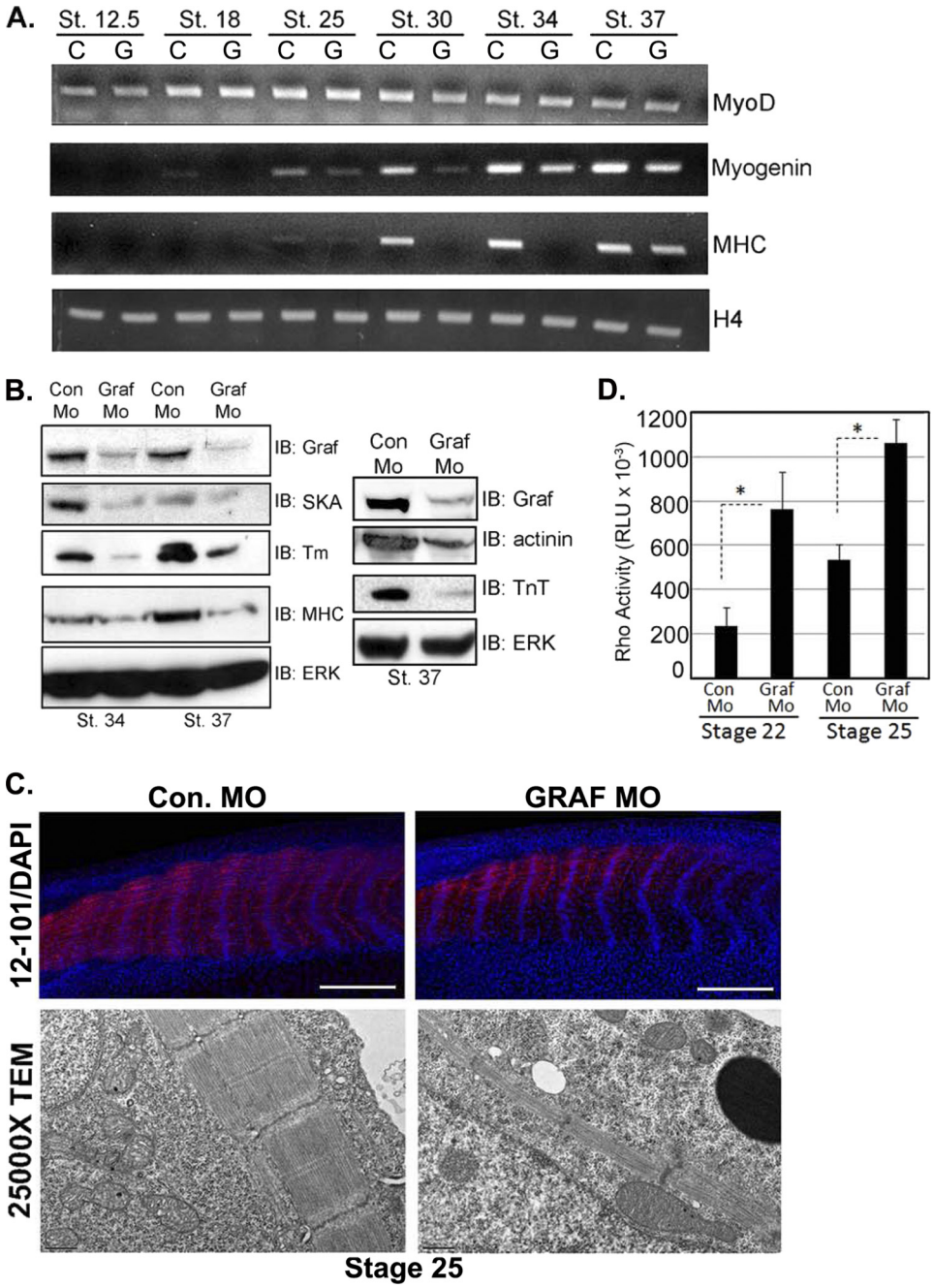

FIGURE 12. **GRAF1 morphants exhibit elevated RhoA activity and impaired skeletal muscle differentiation.** *A,* RNA from Con Mo (*C*)- and GRAF1 Mo (*G*)-injected embryos ($n = 10$) was isolated and utilized for semi-quantitative RT-PCR analysis of indicated marker gene. *B,* lysates from Con Mo- and GRAF1 Mo-injected embryos at the indicated stages were analyzed by Western analysis. Note that the lysates shown in the *left panel* are identical to those shown in Fig. 2*A*. Lysates used for *right panel* were collected from a separate experiment. *IB*, immunoblot. *C, top,* laser scanning confocal microscopy of whole-mount 12–101 (*red*) and ToPro3 (*blue*)-stained stage 25 Con Mo- and GRAF1 Mo-injected embryos (*scale bar,* 500 μm). Note appropriate alignment of nuclei but reduced skeletal muscle differentiation (also see Fig. S3, *A* and *B* and Table 1). *Bottom,* TEM (×2500 magnification) from somite-matched stage 25 Con Mo- and GRAF1 Mo-injected embryo. Note reduced myofiber content in GRAF1 morphants relative to controls. *D,* ELISA-based RhoA activity assays were performed on lysates isolated from stage 22 and 25 Con Mo- and GRAF1 Mo-injected embryos. Ten embryos were processed in batch for each stage and treatment.

scripts were observed between Con Mo- and GRAF1 MO-injected embryos from stages 12.5 to 34 (Fig. 12*A*), indicating that dystrophic phenotypes observed in the GRAF1 morphants are not a consequence of defective specification of the pre-somitic mesoderm.

During *Xenopus* somitogenesis, somitic cells undergo a 90° rotation relative to the anteroposterior axis to form parallel myotome fibers that attach to myosepta (35). To determine whether this morphogenetic step was altered in the GRAF1 morphants, we next stained stage 25 embryos with ToPro3 (nuclear stain) and a panel of muscle and/or myoseptal boundary markers. Confocal views through the myotome revealed that GRAF1 morphant embryos contain nuclei that are arranged in a regularly ordered fashion and are aligned along the dorsoventral axis at the mid-point of each somite block (supplemental Fig. S8*A*), indicating that the GRAF1 morphant

TABLE 1

GRAF1 depletion leads to progressive somite degeneration

Data represent 25–33 embryos for both control and GRAF morphants per time point from 4 experiments.

Dystrophic phenotype	Stage 25–30	Stage 32–34	Stage 37–39
	%	%	%
Discontinuous boundaries	12	87	100
Muscle tears			
Minor	0	13	100
Moderate	0	51	0
Severe	0	36	0
Lack of segmental organization	0	36	100

cells completed the 90° rotation that is necessary for subsequent attachment to the myosepta. Moreover, the levels and continuity of laminin at repetitive intersomitic boundary units were comparable between control and the majority of GRAF1 morpholino-injected embryos at stage 25 (22/25; supplemental Fig. S8*A* and Table 1). Although a small percentage (3/25 GRAF1 morphants) exhibited mild myoseptal disruptions (see supplemental Fig. S8*B* for representative image), co-staining with an antibody that recognizes the C terminus of β-dystroglycan revealed a continuous overlay of β-dystroglycan and laminin in all control MO and GRAF1 Mo-injected embryos, indicating that somitic cells are appropriately anchored to the intersomitic junctions by stage 25 (supplemental Fig. S8*A*). Co-staining with laminin and antibodies that recognize focal adhesion complex proteins, including paxillin (supplemental Fig. S8), vinculin, and FAK (data not shown), confirmed that the GRAF1 morphant somitic cells are aligned parallel to the notochord and establish appropriate anchoring to the extracellular matrix at the intersomitic boundaries. Thus, the initial specification, rotation, and attachment of somitic cells to the myoseptum appear to be largely unaffected in the GRAF1 morphants.

GRAF1 Is Necessary for Skeletal Muscle Differentiation/Maturation in Developing Tadpoles—Based on our studies in C2C12 cells, we reasoned that the muscle degeneration phenotype might have resulted from impaired skeletal muscle maturation (the next step of somitogenesis). To address this hypothesis, we first analyzed Con Mo- and GRAF1 Mo-injected embryos by semi-quantitative RT-PCR analysis for the skeletal muscle differentiation markers, myogenin and skeletal muscle myosin heavy chain. As shown in Fig. 12*A*, myogenin and MHC transcripts were lower in GRAF1-depleted embryos in comparison with the Con Mo-injected controls from stage 18 to 34. These findings were confirmed by Western blotting of whole-embryo lysates. GRAF1 depletion led to decreased expression of all differentiation markers evaluated, including MHC, Tm, SKA, α-actinin, and troponin T (Fig. 12*B*). Accordingly, dual labeling of stage 25 embryos with the early skeletal muscle differentiation marker 12-101 (36) revealed much lower levels of skeletal muscle maturation marker in GRAF1 morphant somites relative to controls (Fig 12*C*, *top panel*). Moreover, using a luminescence-based assay to quantify the GTP-bound form of RhoA, we found that RhoA activity was significantly increased in GRAF1 MO-injected embryos compared with Con MO-injected embryos at the onset of skeletal muscle differentiation (*stages 22* and *25*; Fig. 12*D*). These data confirm our previous findings that GRAF1 acts as a *bona fide* Rho-GAP *in vivo* and further extends these findings by demonstrating that GRAF1 serves to down-regulate Rho activity during critical stages of muscle development.

Ultrastructural analysis by transmission electron microscopy confirmed a marked reduction in myofiber content as exemplified by more sarcoplasm and less myofibers per myocyte in GRAF1 morphant somites relative to somite-matched controls at both stage 25 (Fig. 12*C*, *bottom*) and 37 (Fig. 11*B*). Although repetitive Z-band containing sarcomeres were formed, a lack of M-bands was apparent, consistent with the marked reduction of MHC. Thus, we conclude that GRAF plays a critical and conserved role in promoting muscle fiber maturation and that the deterioration of muscle and myoseptal boundaries observed at later stages in the GRAF morphants is likely due to the inability of the malformed muscle fibers to withstand the mechanical strain imparted on them during subsequent development and/or induction of motility.

DISCUSSION

Recent studies suggest that down-regulation of RhoA is required for skeletal muscle differentiation and myotube fusion; however, little is known about the importance of this mechanism *in vivo* or about the molecules that limit RhoA activity during skeletal muscle development. We show for the first time that the Rho-specific GAP, GRAF1, is required for proper skeletal muscle differentiation and sarcomere formation in *X. laevis.* Importantly, mammalian GRAF1 is also highly up-regulated during skeletal muscle maturation, and GRAF1-dependent down-regulation of Rho activity was necessary and sufficient for skeletal muscle differentiation in the C2C12 model. Moreover, localization of GRAF1 to cell junctions also facilitated myoblast fusion into multinucleated myotubes, and this effect required GRAF1 GAP and BAR domains. Collectively, these data support a cell autonomous and conserved role for GRAF1 in the control of myogenesis and provide novel insight into coordinated actin- and membrane-based mechanisms that regulate myotube fusion.

GRAF1 morphant tadpoles exhibited a highly penetrant swimming defect that was accompanied by disrupted somite structure, a curved body axis, and low motor activity. Although examples of severe cellular and myoseptal disruptions were found in all the regions of stage 34–37 GRAF1 morphant embryos, the middle region was most severely affected. This phenotype differs from integrin α5 subunit depletion, which leads to restricted defects in anterior somites (37, 38). Interestingly, disruption of β-dystroglycan or integrin-linked kinase in these species led to similar gross morphological defects and as those observed in our GRAF1 morphants (39–41). However, the cause for fiber degeneration is distinct as depletion of integrin-linked kinase resulted in detachment of the intact cell from the matrix (39), whereas depletion of β-dystroglycan led to detachment within the sarcolemmal membrane plane (40, 41), and depletion of GRAF1 led to severing of the contractile units.

In some cases, attachment failure in GRAF1 morphants occurred within the extracellular matrix itself, because laminin was found to retract into the myotome with the fiber (similar to what was observed in zebrafish containing a mutation in the laminin α2 gene (42)). Although it is difficult to distinguish the etiology of the matrix defect in the GRAF1 morphants, it is

possible that initial impairment in the differentiation and tension generation of the myofibers could lead to impaired integrin inside-out signaling and subsequent loss of matrix cohesiveness (43, 44). The findings that the initial deposition and organization of matrix are normal in the majority of GRAF1 morphants and that the GRAF1 morphants are capable of remodeling the laminin matrix to ensure reattachment of presumptive regenerating fibers with the myoseptum (apparent in later stage embryos) indicate that defective myofibrillogenesis is likely the primary cause of myoseptal boundary deterioration observed in the more severe cases. Thus, we surmise that the lack of appropriate myofiber production renders the cells vulnerable to growth-, contraction-, or twitching-induced mechanical damage to the contractile apparatus, which leads to fiber retraction and subsequent degeneration of the myoseptal extracellular matrix. This thesis is consistent with enhanced severity in the middle of the embryo, which exhibits the most torsion upon twitching or induction of motility. Although our studies clearly show that GRAF1 regulates skeletal muscle differentiation, a role for GRAF1 in regulating myoblast fusion *in vivo* could not be assessed in the *Xenopus* model, because all GRAF morphants died prior to the induction of this process.

There are intriguing similarities, yet some differences between the reported effects of FAK on somite morphogenesis, muscle differentiation, and fusion and the effects of GRAF1 reported herein. With respect to somitogenesis, Kragtorp and Miller (14) reported that ectopic expression of the FAK inhibitor, FRNK, led to early defects in somite rotation associated with impaired fibronectin matrix deposition and assembly. Our data indicate that GRAF1 is expressed at low levels during these early stages and that GRAF1 depletion does not impair somite rotation, indicating that FAK likely acts through different targets to regulate these early events. Indeed, data presented by Kragtorp and Miller (14) indicate that FAK acts in concert with Ena/VASP proteins to modulate integrin activity and integrin-extracellular matrix interactions that are necessary for the movement of cells prior to alignment with the myoseptum. Interestingly, recent studies indicate that FAK may also function to regulate later myogenic processes, because FAK is required for myogenin expression, terminal differentiation, and fusion of cultured myoblasts (17, 45). These findings are reminiscent of the functions of GRAF1 in these cells and indicate that GRAF1 may aid to mediate these later FAK-dependent effects. In support of this possibility, we found that an SH3-binding mutant of GRAF1 (that fails to interact with FAK) has a limited capacity to induce skeletal muscle differentiation, indicating that FAK might regulate the appropriate localization and function of GRAF1. Future studies will further address the requirement for the FAK-GRAF1 interaction in muscle development.

Clearly, a complex array of guanine nucleotide exchange proteins and GAPs provides tight control of GTPase activity during the many critical stages of muscle development (9). Our report is the first to demonstrate a role for GRAF1 in the spatial and temporal down-regulation of Rho during skeletal muscle maturation and fusion. Although no other GAPs have been identified that regulate muscle maturation, previous studies have shown that p190B Rho-GAP expression in mesenchymal cells favors adipocyte specification over myogenic specification (10). Although MyoD expression is initiated prior to marked depletion of GRAF1 in our model, the findings that depletion of GRAF1 from stage 18 onward had no effect on MyoD levels or localization throughout development and that GRAF1 expression in mammalian muscle occurs much later than myoblast specification suggest that GRAF1 does not affect muscle specification. Thus, these two RhoA-specific GAPs appear to have nonoverlapping roles during early and late stages of muscle differentiation, respectively, although it will be important to further define their expression patterns, cellular localizations, and overall activity during muscle development.

Our finding that GRAF1 promoted skeletal muscle differentiation is consistent with previous reports demonstrating that inhibition of Rho/ROCK signaling in differentiating myocytes promoted expression of skeletal muscle marker genes and induced terminal differentiation (3, 4). However, these data seem at odds with the known function of Rho to stimulate the serum-response factor-dependent expression of many muscle-specific genes (46) by enhancing the nuclear localization of the myocardin-related serum-response co-factors. This discrepancy may be explained by the recent demonstration that RhoA-dependent activation of MRTF-A in proliferating myoblasts induced the expression of the helix-loop-helix transcriptional inhibitor, Id3 and that depletion of Id3 in these proliferating cells induced terminal differentiation (4).

We also found that temporal induction of GRAF1 (but not GAPm) in pre-differentiated myoblasts induced marked fusion into multinucleated myotubes. Recent elegant time-lapse imaging of fusing myoblasts revealed that pre-fused cells assume a bipolar shape that is induced by the interaction of nonmuscle myosin 2A with actin at the plasma membrane and that a focus of F-actin appears at the future site of myoblast fusion (7, 47). The findings that mutations in known fusion genes such as *kette*, *mbc*, and *SCAR/WAVE* all lead to enlarged F-actin foci that fail to dissolve indicate that both the formation and subsequent dissolution of this actin focus is essential for myoblast fusion (48, 49). Rho has been shown to initiate actin polymerization at the onset of the protrusion-retraction cycle, by activating members of the formin family such as mDia (50, 51). Thus, we reasoned that GRAF1 might limit Rho-dependent actin polymerization at sites of myoblast fusion. In support of this theory, we have shown that GRAF1 localizes to the tips of pre-fused bipolar myoblasts at the inner face of actin-based processes, thereby placing its catalytic activity in close proximity to the actin focus. Moreover, myoblasts in which GRAF1 is overexpressed exhibit much smaller actin foci than control cells or those expressing GAPm, indicating that GRAF1 promotes dissolution of the actin focus. Recruitment of GRAF1 from the perinuclear region (as is observed in proliferating myoblasts) to leading edge protrusions could thus represent a necessary step for limiting Rho-dependent actin polymerization during myoblast fusion.

We also identified a completely novel role for the GRAF1 BAR domain in regulating myoblast fusion. Unlike the GRAF1 GAP domain, which is necessary for both differentiation and fusion, the BAR domain is only required for myoblast fusion. We found that the BAR domain of GRAF1 was dispensable for

recruitment of GRAF1 to the bipolar tips of pre-fused myoblasts, suggesting that the BAR domain may mediate a critical membrane sculpting function. Structural analysis indicates that BAR domains form elongated homodimers characterized by a shallow curvature formed by the anti-parallel interaction of two α-helical coils that facilitate membrane deformation (52). Although our studies are the first to identify a BAR domain-containing protein as a critical mediator of skeletal muscle fusion, these lipid bending domains have been previously implicated in both promoting secretory vesicle fission to (and endocytic vesicle budding from) plasma membranes. Indeed, the GRAF1 BAR domain is capable of inducing tubulation of spherical lipids and has been implicated in driving clathrin-independent endocytosis in fibroblasts and HeLa cells (29, 30). Interestingly, other mediators of endocytic membrane recycling, including myoferlin, MG53, and Eps15 homology domain-containing proteins 1 and 2, have recently been shown to promote myoblast fusion (31–33). The presence of unilamellar vesicles observed at sites of myoblast membrane fusion has been proposed to be important for the recruitment of essential fusogenic phospholipids and the subsequent internalization of excess plasma membrane from fusing cells (34). However, to what extent the specific clathrin-independent/glycosylphosphatidylinositol-enriched endocytic compartments that are regulated by GRAF1 might facilitate this process is unknown. It is also possible that the GRAF1 BAR domain may act in a similar fashion to some BAR domain-containing proteins (such as the related F-BAR containing Rho-GAP, srGAP2) by binding to the inner neck of the membrane protrusion to induce outward membrane curvature (53). In fusion-competent cells, such an event could result in enhanced hydrophobic attractions between the interiors of the two bilayers, thus promoting lipid transfer from one membrane to another (54, 55). We have found that GRAF1 localizes to the base of dorsal ruffles (circular ruffles that project up from the plasma membrane; see supplemental Fig. S2*A*) and that ectopic expression of GRAF1 induces numerous membrane protrusions in myoblasts (see supplemental Fig. S2*B*). Hence, we speculate that in skeletal muscle, GRAF1 (and perhaps other BAR domain-containing proteins) might operate to facilitate the initial steps of myotube formation by bringing membranes from two apposed myoblasts into direct contact. Whether GRAF1 serves to promote myoblast fusion by enhancing membrane interactions via membrane sculpting and/or by regulating endocytic recycling are interesting questions for future studies.

In summary, we provide the first evidence that induction of skeletal muscle differentiation is a fundamental GRAF1-dependent process that is conserved across species. The progressive myofiber degeneration observed in the *Xenopus* GRAF1 morphants resembles several models of congenic muscular dystrophies and highlights a possible role for persistent Rho activation in the pathogenesis of this disease. This study also furthers our understanding of the coordinated control of cytoskeletal and membrane processes during myotube fusion. The mechanisms by which GRAF1 or other BAR domain-containing proteins impact mammalian myotube formation and/or muscle repair following injury are exciting questions for future study.

REFERENCES

1. Chargé, S. B., and Rudnicki, M. A. (2004) *Physiol. Rev.* **84,** 209–238
2. Bryan, B. A., Mitchell, D. C., Zhao, L., Ma, W., Stafford, L. J., Teng, B. B., and Liu, M. (2005) *Mol. Cell. Biol.* **25,** 11089–11101
3. Castellani, L., Salvati, E., Alemà, S., and Falcone, G. (2006) *J. Biol. Chem.* **281,** 15249–15257
4. Iwasaki, K., Hayashi, K., Fujioka, T., and Sobue, K. (2008) *J. Biol. Chem.* **283,** 21230–21241
5. Charrasse, S., Comunale, F., Grumbach, Y., Poulat, F., Blangy, A., and Gauthier-Rouvière, C. (2006) *Mol. Biol. Cell* **17,** 749–759
6. Benezra, R., Davis, R. L., Lockshon, D., Turner, D. L., and Weintraub, H. (1990) *Cell* **61,** 49–59
7. Peckham, M. (2008) *J. Microsc.* **231,** 486–493
8. Swailes, N. T., Knight, P. J., and Peckham, M. (2004) *J. Anat.* **205,** 381–391
9. Tcherkezian, J., and Lamarche-Vane, N. (2007) *Biol. Cell* **99,** 67–86
10. Sordella, R., Jiang, W., Chen, G. C., Curto, M., and Settleman, J. (2003) *Cell* **113,** 147–158
11. Hildebrand, J. D., Taylor, J. M., and Parsons, J. T. (1996) *Mol. Cell. Biol.* **16,** 3169–3178
12. Taylor, J. M., Macklem, M. M., and Parsons, J. T. (1999) *J. Cell Sci.* **112,** 231–242
13. Taylor, J. M., Hildebrand, J. D., Mack, C. P., Cox, M. E., and Parsons, J. T. (1998) *J. Biol. Chem.* **273,** 8063–8070
14. Kragtorp, K. A., and Miller, J. R. (2006) *Development* **133,** 685–695
15. Henry, C. A., Crawford, B. D., Yan, Y. L., Postlethwait, J., Cooper, M. S., and Hille, M. B. (2001) *Dev. Biol.* **240,** 474–487
16. Quach, N. L., and Rando, T. A. (2006) *Dev. Biol.* **293,** 38–52
17. Luo, S. W., Zhang, C., Zhang, B., Kim, C. H., Qiu, Y. Z., Du, Q. S., Mei, L., and Xiong, W. C. (2009) *EMBO. J.* **28,** 2568–2582
18. DiMichele, L. A., Hakim, Z. S., Sayers, R. L., Rojas, M., Schwartz, R. J., Mack, C. P., and Taylor, J. M. (2009) *Circ. Res.* **104,** 1201–1208
19. Wilson, L., Carrier, M. J., and Kellie, S. (1995) *J. Cell Sci.* **108,** 2381–2391
20. Liu, K. J., and Harland, R. M. (2003) *Dev. Biol.* **264,** 339–351
21. Goetz, S. C., Brown, D. D., and Conlon, F. L. (2006) *Development* **133,** 2575–2584
22. Meadows, S. M., Warkman, A. S., Salanga, M. C., Small, E. M., and Krieg, P. A. (2008) *Proc. Natl. Acad. Sci. U.S.A.* **105,** 1545–1550
23. Small, E. M., Warkman, A. S., Wang, D. Z., Sutherland, L. B., Olson, E. N., and Krieg, P. A. (2005) *Development* **132,** 987–997
24. Benard, V., Bohl, B. P., and Bokoch, G. M. (1999) *J. Biol. Chem.* **274,** 13198–13204
25. Jansen, K. M., and Pavlath, G. K. (2008) *Methods Mol. Biol.* **475,** 115–133
26. Blau, H. M., Chiu, C. P., Pavlath, G. K., and Webster, C. (1985) *Adv. Exp. Med. Biol.* **182,** 231–247
27. Yaffe, D. (1968) *Proc. Natl. Acad. Sci. U.S.A.* **61,** 477–483
28. Halevy, O., Novitch, B. G., Spicer, D. B., Skapek, S. X., Rhee, J., Hannon, G. J., Beach, D., and Lassar, A. B. (1995) *Science* **267,** 1018–1021
29. Lundmark, R., Doherty, G. J., Howes, M. T., Cortese, K., Vallis, Y., Parton, R. G., and McMahon, H. T. (2008) *Curr. Biol.* **18,** 1802–1808
30. Eberth, A., Lundmark, R., Gremer, L., Dvorsky, R., Koessmeier, K. T., McMahon, H. T., and Ahmadian, M. R. (2009) *Biochem. J.* **417,** 371–377
31. Doherty, K. R., Demonbreun, A. R., Wallace, G. Q., Cave, A., Posey, A. D., Heretis, K., Pytel, P., and McNally, E. M. (2008) *J. Biol. Chem.* **283,** 20252–20260
32. Cai, C., Masumiya, H., Weisleder, N., Pan, Z., Nishi, M., Komazaki, S., Takeshima, H., and Ma, J. (2009) *J. Biol. Chem.* **284,** 3314–3322
33. Posey, A. D., Jr., Pytel, P., Gardikiotes, K., Demonbreun, A. R., Rainey, M., George, M., Band, H., and McNally, E. M. (2011) *J. Biol. Chem.* **286,** 7379–7388
34. Kalderon, N., and Gilula, N. B. (1979) *J. Cell Biol.* **81,** 411–425
35. Keller, R. (2000) *Curr. Top. Dev. Biol.* **47,** 183–246
36. Kintner, C. R., and Brockes, J. P. (1984) *Nature* **308,** 67–69
37. Koshida, S., Kishimoto, Y., Ustumi, H., Shimizu, T., Furutani-Seiki, M., Kondoh, H., and Takada, S. (2005) *Dev. Cell.* **8,** 587–598
38. Kragtorp, K. A., and Miller, J. R. (2007) *Dev. Dyn.* **236,** 2713–2720
39. Postel, R., Vakeel, P., Topczewski, J., Knöll, R., and Bakkers, J. (2008) *Dev. Biol.* **318,** 92–101

40. Hidalgo, M., Sirour, C., Bello, V., Moreau, N., Beaudry, M., and Darribère, T. (2009) *Dev. Dyn.* **238,** 1332–1345
41. Jacoby, A. S., Busch-Nentwich, E., Bryson-Richardson, R. J., Hall, T. E., Berger, J., Berger, S., Sonntag, C., Sachs, C., Geisler, R., Stemple, D. L., and Currie, P. D. (2009) *Development* **136,** 3367–3376
42. Hall, T. E., Bryson-Richardson, R. J., Berger, S., Jacoby, A. S., Cole, N. J., Hollway, G. E., Berger, J., and Currie, P. D. (2007) *Proc. Natl. Acad. Sci. U.S.A.* **104,** 7092–7097
43. Rooney, J. E., Welser, J. V., Dechert, M. A., Flintoff-Dye, N. L., Kaufman, S. J., and Burkin, D. J. (2006) *J. Cell Sci.* **119,** 2185–2195
44. Chong, S. W., and Jiang, Y. J. (2005) *Trends Cell Biol.* **15,** 453–457
45. Quach, N. L., Biressi, S., Reichardt, L. F., Keller, C., and Rando, T. A. (2009) *Mol. Biol. Cell* **20,** 3422–3435
46. Puri, P. L., and Sartorelli, V. (2000) *J. Cell. Physiol.* **185,** 155–173
47. Duan, R., and Gallagher, P. J. (2009) *Dev. Biol.* **325,** 374–385
48. Schröter, R. H., Lier, S., Holz, A., Bogdan, S., Klämbt, C., Beck, L., and Renkawitz-Pohl, R. (2004) *Development* **131,** 4501–4509
49. Schäfer, G., Weber, S., Holz, A., Bogdan, S., Schumacher, S., Müller, A., Renkawitz-Pohl, R., and Onel, S. F. (2007) *Dev. Biol.* **304,** 664–674
50. Narumiya, S., Ishizaki, T., and Watanabe, N. (1997) *FEBS Lett.* **410,** 68–72
51. Yamana, N., Arakawa, Y., Nishino, T., Kurokawa, K., Tanji, M., Itoh, R. E., Monypenny, J., Ishizaki, T., Bito, H., Nozaki, K., Hashimoto, N., Matsuda, M., and Narumiya, S. (2006) *Mol. Cell. Biol.* **26,** 6844–6858
52. Henne, W. M., Kent, H. M., Ford, M. G., Hegde, B. G., Daumke, O., Butler, P. J., Mittal, R., Langen, R., Evans, P. R., and McMahon, H. T. (2007) *Structure* **15,** 839–852
53. Suetsugu, S. (2010) *J. Biochem.* **148,** 1–12
54. Marrink, S. J., and Mark, A. E. (2003) *J. Am. Chem. Soc.* **125,** 11144–11145
55. Chanturiya, A., Scaria, P., Kuksenok, O., and Woodle, M. C. (2002) *Biophys. J.* **82,** 3072–3080